

Strange Atoms, Strange Nuclei and Kaon Condensation*

E. Friedman^{1,†} and A. Gal^{1,‡}

¹*Racah Institute of Physics, The Hebrew University, Jerusalem 91904, Israel*

(Dated: February 2, 2008)

Abstract

Analyses of strong-interaction data consisting of level shifts, widths and yields in strange atoms of K^- mesons and Σ^- hyperons are reviewed. Recent results obtained by fitting to comprehensive sets of data across the periodic table in terms of density dependent optical potentials are discussed. The introduction of density dependence generally improves significantly the fit to the data, leading to novel results on the in-medium hadron-nucleon t matrix $t(\rho)$ over a wide range of densities up to central nuclear densities. A strongly attractive K^- -nuclear potential of order 150–200 MeV in nuclear matter is suggested by fits to K^- -atom data, with interesting possible repercussions on \bar{K} condensation and on the evolution of strangeness in high-density stars. The case for relatively narrow deeply bound K^- atomic states is made, essentially independent of the K^- potential depth. In view of the recently reported inconclusive experimental signals of \bar{K} deeply bound states, dynamical models for calculating binding energies and widths of \bar{K} -nuclear states are discussed. Lower bounds on the width, $\Gamma_{\bar{K}} \gtrsim 50$ MeV, are established. For Σ^- atoms, the fitted potential becomes repulsive inside the nucleus, in agreement with recently reported (π^-, K^+) spectra from KEK, implying that Σ hyperons generally do not bind in nuclei. This repulsion significantly affects calculated compositions and masses of neutron stars.

PACS numbers: 13.75.Jz; 21.80.+a; 25.80.Nv; 26.60.+c; 36.10.Gv

Keywords: kaonic atoms; K^- deeply bound atomic and nuclear states; kaon condensation; sigmionic atoms; Σ hypernuclei; neutron stars

* Lectures delivered by Avraham Gal at the International School of Physics Enrico Fermi, Varenna, June 2007.

[†]Electronic address: elifried@vms.huji.ac.il

[‡]Electronic address: avragal@vms.huji.ac.il

Contents

I. Introduction	3
II. Exotic atom methodology	4
A. Wave equations and optical potentials	4
B. Nuclear densities	4
C. Radial sensitivity in exotic atoms	5
D. Nonperturbative aspects of exotic atoms	6
III. K^- Atoms	7
A. Fits to K^- -atom data	7
B. Deeply bound K^- atomic states	10
IV. \bar{K} Nuclear Interactions	12
A. The K^-p interaction near threshold	12
B. \bar{K} -nucleus potentials	14
C. Deeply bound K^- nuclear states in light nuclei	15
D. RMF dynamical calculations of \bar{K} quasibound nuclear states	17
E. Kaon condensation	19
V. Σ Hyperons	20
A. Overview	20
B. Fits to Σ^- atoms	22
C. Evidence from (π^-, K^+) spectra	25
Acknowledgments	27
References	27

I. INTRODUCTION

An exotic atom is formed when a negatively charged particle stops in a target and is captured by a target atom into an outer atomic orbit. It will then emit Auger electrons and characteristic X-rays whilst cascading down its own sequence of atomic levels until, at some state of low principal quantum number n , the particle is absorbed due to its interaction with the nucleus. The lifetimes of the particles considered here, namely K^- and Σ^- , are much longer than typical slowing down times and atomic time scales. Therefore, following the stopping of the hadron in matter, well defined states of an exotic atom are established and the effects of the hadron-nucleus strong interaction can be studied. The overlap of the atomic orbitals with the nucleus covers a wide range of nuclear densities thus creating a unique source of information on the density dependence of the hadronic interaction.

In the study of strong interaction effects in exotic atoms, the observables of interest are the shifts (ϵ) and widths (Γ) of the atomic levels caused by the strong interaction with the nucleus. These levels are shifted and broadened relative to the electromagnetic case but the shifts and widths can usually only be measured directly for one, or possibly two levels in any particular hadronic atom. The broadening due to the nuclear absorption usually terminates the atomic cascade at low n thus limiting the experimentally observed X-ray spectrum. In some cases the width of the next higher $n + 1$ ‘upper’ level can be obtained indirectly from measurements of the relative yields of X-rays when they depart from their purely electromagnetic values. As the atomic number and size of the nucleus increase, so the absorption occurs from higher n -values as shown for K^- atoms and for Σ^- atoms in the corresponding Sections. Shifts and widths caused by the interaction with the nucleus may be calculated by adding an optical potential to the Coulomb interaction. The study of the strong interaction in exotic atoms thus becomes the study of this additional potential, as reviewed in great detail by Batty, Friedman and Gal [1] and very recently by Friedman and Gal [2]. On the experimental side, studies of strong interaction effects in exotic atoms have been transformed over the years with the introduction of increasingly more advanced X-ray detectors and with increasing the efficiency of stopping the hadrons, such as with a cyclotron trap [3].

The present Lectures focus particularly on the physics of the strong interaction which can be deduced by studying strange atoms, a term which is used for exotic atoms formed initially by stopping K^- mesons in matter. The importance of the Strange Atoms subject stems from the progress made in recent years in quantifying medium modification effects on the hadron-nucleus interaction which has enabled one to achieve improved fits to existing data within the framework of commonly accepted models [2]. These modified interactions obey a low density limit which has not always been enforced in earlier analyses, since it is not always relevant to the higher density regime explored, where new features of the hadron nucleus interaction may become significant to other fields such as astrophysics.

In the next section we will outline the methodology of exotic-atom studies, including common tools such as wave equations and optical potentials. Of prime importance is the dependence of the optical potential on the model of nuclear density used, with emphasis placed on the overlap region between the atomic state studied and the nucleus. Radial sensitivity will be defined, to serve as a guide. Finally the extreme non perturbative nature of exotic atoms will be discussed. Readers who are not concerned about these tools of analyzing exotic atoms may skip the next section and go immediately to the sections dealing with K^- atoms and nuclei and with Σ hyperons.

II. EXOTIC ATOM METHODOLOGY

A. Wave equations and optical potentials

The interaction of hadrons at threshold with the nucleus is customarily described by a Klein-Gordon (KG) equation which for exotic-atom applications is of the following form:

$$\left[\nabla^2 - 2\mu(B + V_{\text{opt}} + V_c) + (V_c + B)^2 \right] \psi = 0 \quad (\hbar = c = 1) \quad (1)$$

where μ is the hadron-nucleus reduced mass, B is the complex binding energy and V_c is the finite-size Coulomb interaction of the hadron with the nucleus, including vacuum-polarization terms, added according to the minimal substitution principle $E \rightarrow E - V_c$. A term $2V_c V_{\text{opt}}$ and a term $2B V_{\text{opt}}$ were neglected in Eq. (1) with respect to $2\mu V_{\text{opt}}$; the term $2B V_{\text{opt}}$ has to be reinstated in studies of deeply-bound states. The optical potential V_{opt} is of the $t\rho(r)$ generic class which for underlying s -wave hadron-nucleon interactions assumes the form:

$$2\mu V_{\text{opt}}(r) = -4\pi \left(1 + \frac{A-1}{A} \frac{\mu}{M} \right) \{ b_0 [\rho_n(r) + \rho_p(r)] + \tau_z b_1 [\rho_n(r) - \rho_p(r)] \}. \quad (2)$$

Here, ρ_n and ρ_p are the neutron and proton density distributions normalized to the number of neutrons N and number of protons Z , respectively, M is the mass of the nucleon and $\tau_z = +1$ for the negatively charged hadrons considered in the present Lectures. In the impulse approximation, b_0 and b_1 are minus the hadron-nucleon isoscalar and isovector scattering lengths, respectively, which are complex for the absorptive strong interactions of K^- mesons and Σ^- hyperons. Generally these ‘one-nucleon’ parameters are functions of the density ρ , but often the density dependence may be approximated by fitting effective values for b_0 and b_1 to low-energy data. The extension of the threshold KG equation (1) and the optical potential (2) for scattering problems is straightforward [1, 2].

The use of the KG equation rather than the Dirac equation for Fermions, such as Σ hyperons, is numerically justified when fine-structure effects are negligible or are treated in an average way, as for the X-ray transitions considered here. The leading j dependence ($j = l \pm \frac{1}{2}$) of the energy for solutions of the Dirac equation for a point-charge $1/r$ potential goes as $(j + \frac{1}{2})^{-1}$, and on averaging it over the projections of j gives rise to $(l + \frac{1}{2})^{-1}$ which is precisely the leading l dependence of the energy for solutions of the KG equation. The higher-order contributions to the spin-orbit splitting are suppressed by $O(Z\alpha/n)^2$ which is of order 1% for the high- n X-ray transitions encountered for Σ hyperons. This is considerably smaller than the experimental errors placed on the measured X-ray transition energies and widths.

B. Nuclear densities

The nuclear densities are an essential ingredient of the optical potential. The density distribution of the protons is usually considered known as it is obtained from the nuclear charge distribution by unfolding the finite size of the charge of the proton. The neutron distributions are, however, generally not known to sufficient accuracy. For many nuclei there is no direct experimental information whatsoever on neutron densities and one must then rely on models which sometimes give conflicting results for the root-mean-square (rms)

radii. Given this unsettled state of affairs, a semi-phenomenological approach was adopted that covers a broad range of possible neutron density distributions.

Experience with pionic atoms showed [2] that the feature of neutron density distributions which is most relevant in determining strong interaction effects in pionic atoms is the radial extent, as represented e.g. by r_n , the neutron density rms radius. A linear dependence of $r_n - r_p$ on $(N - Z)/A$ has been successfully employed in \bar{p} studies [4, 5, 6], namely

$$r_n - r_p = \gamma \frac{N - Z}{A} + \delta , \quad (3)$$

with γ close to 1.0 fm and δ close to zero. Expression (3) has been adopted in analyzing strange atoms and, for lack of better global information about neutron densities, the value of γ was varied over a reasonable range in fitting to the data. This procedure is based on the expectation that for a large data set over the whole of the periodic table some local variations will cancel out and that an average behavior may be established. Phenomenological studies of in-medium nuclear interactions are based on such averages.

In order to allow for possible differences in the shape of the neutron distribution, a two-parameter Fermi (2pF) distribution was used both for the known proton (unfolded from the charge distribution) and for the unknown neutron density distributions

$$\rho_{n,p}(r) = \frac{\rho_{0n,0p}}{1 + \exp((r - R_{n,p})/a_{n,p})} , \quad (4)$$

in the ‘skin’ form of Ref. [4]. In this form, the same diffuseness parameter for protons and neutrons, $a_n = a_p$, is assumed and the R_n parameter is determined from the rms radius r_n deduced from Eq. (3) where r_p is considered to be known. It was checked that for K^- atoms and for Σ^- atoms the assumption of ‘skin’ form was as good, or better, than assuming other (notably ‘halo’) forms.

Another sensitivity that may be checked in global fits is to the radial extension of the hadron-nucleon interaction when folded together with the nuclear density. The resultant ‘finite range’ density is defined as

$$\rho^F(r) = \int d\mathbf{r}' \rho(\mathbf{r}') \frac{1}{\pi^{3/2} \beta^3} e^{-(\mathbf{r}-\mathbf{r}')^2/\beta^2} , \quad (5)$$

assuming a Gaussian interaction. It was found that K^- and Σ^- atoms do not display sensitivity to finite-range effects.

C. Radial sensitivity in exotic atoms

The radial sensitivity of exotic atom data was addressed before [1] with the help of a ‘notch test’, introducing a local perturbation into the potential and studying the changes in the fit to the data as function of position of the perturbation. The results gave at least a semi-quantitative information on what are the radial regions which are being probed by the various types of exotic atoms. However, the radial extent of the perturbation was somewhat arbitrary and only very recently that approach was extended [7] into a mathematically well-defined limit.

In order to study the radial sensitivity of *global* fits to exotic atom data, it is necessary to define the radial position parameter globally using as reference, e.g. the known charge

distribution for each nuclear species in the data base. The radial position r is then defined as $r = R_c + \eta a_c$, where R_c and a_c are the radius and diffuseness parameters, respectively, of a 2pF charge distribution [8]. In that way η becomes the relevant radial parameter when handling together data for several nuclear species along the periodic table. The value of χ^2 is regarded now as a functional of a global optical potential $V(\eta)$, i.e. $\chi^2 = \chi^2[V(\eta)]$, where the parameter η is a *continuous* variable. It leads to [7]

$$d\chi^2 = \int d\eta \frac{\delta\chi^2}{\delta V(\eta)} \delta V(\eta), \quad (6)$$

where

$$\frac{\delta\chi^2[V(\eta)]}{\delta V(\eta')} = \lim_{\sigma \rightarrow 0} \lim_{\epsilon_V \rightarrow 0} \frac{\chi^2[V(\eta) + \epsilon_V \delta_\sigma(\eta - \eta')] - \chi^2[V(\eta)]}{\epsilon_V} \quad (7)$$

is the functional derivative (FD) of $\chi^2[V]$. The notation $\delta_\sigma(\eta - \eta')$ stands for an approximated δ -function and ϵ_V is a change in the potential. From Eq. (6) it is seen that the FD determines the effect of a local change in the optical potential on χ^2 . Conversely it can be said that the optical potential sensitivity to the experimental data is determined by the magnitude of the FD. Calculation of the FD may be carried out by multiplying the best fit potential by a factor

$$f = 1 + \epsilon \delta_\sigma(\eta - \eta') \quad (8)$$

using a normalized Gaussian with a range parameter σ for the smeared δ -function,

$$\delta_\sigma(\eta - \eta') = \frac{1}{\sqrt{2\pi}\sigma} e^{-(\eta - \eta')^2 / 2\sigma^2}. \quad (9)$$

For finite values of ϵ and σ the FD can then be approximated by

$$\frac{\delta\chi^2[V(\eta)]}{\delta V(\eta')} \approx \frac{1}{V(\eta')} \frac{\chi^2[V(\eta)(1 + \epsilon \delta_\sigma(\eta - \eta'))] - \chi^2[V(\eta)]}{\epsilon}. \quad (10)$$

The parameter ϵ is used for a *fractional* change in the potential and the limit $\epsilon \rightarrow 0$ is obtained numerically for several values of σ and then extrapolated to $\sigma = 0$.

D. Nonperturbative aspects of exotic atoms

The optical potentials used to calculate the shifts and widths of atomic energy levels are confined to a small region of the atom and thus lead to very small energy shifts compared to the corresponding binding energies. However, they greatly modify the wavefunction locally and this modification makes the strong interaction effects non-perturbative. For example, in kaonic atoms all the measured level shifts are repulsive, yet ' $t_{\text{eff}}\rho$ ' fits to the data invariably lead to attractive potentials. The net repulsive shift is due to the imaginary part of the potential being comparable in magnitude to the real part. Repulsive shifts may also arise from dominantly real attractive optical potentials that are sufficiently strong to bind *nuclear* states. A nuclear state generated by the optical potential gives rise to a node inside the nucleus for the atomic wavefunction by orthogonality. The strong modification of atomic wavefunctions due to binding nuclear states by V_{opt} may also give rise to irregularities in the parameters of V_{opt} obtained from fits to data. This effect was first observed by Krell [9] for kaonic atoms. These irregularities can be explained by large variations in the atomic wavefunctions such that additional nodes may be accommodated within the nucleus. A more comprehensive discussion of these nonperturbative aspects is found in Ref. [10].

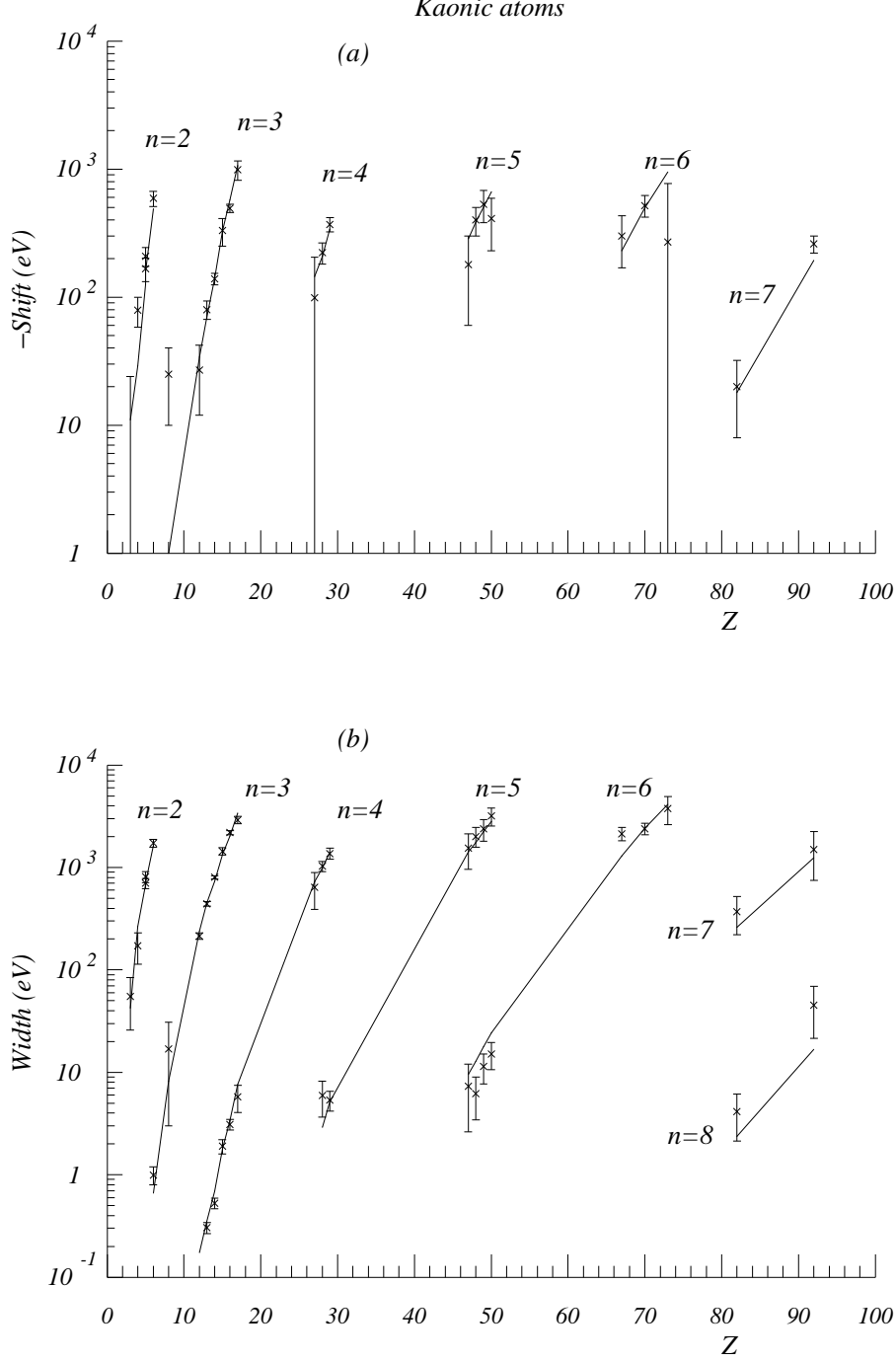


FIG. 1: Shift and width values for kaonic atoms. The continuous lines join points calculated with a best-fit DD optical potential.

III. K^- ATOMS

A. Fits to K^- -atom data

The K^- -atom data used in global fits [1] are shown in Fig. 1, spanning a range of atomic states from $2p$ in Li to $8j$ in U, with 65 level-shifts, widths and transition yields data

points. We note that the shifts are ‘repulsive’, largely due to the substantial absorptivity of the K^- -nuclear interaction. It was shown already in the mid 1990s [1] that although a reasonably good fit to the data is obtained for a $t\rho$ potential, Eq. (2), with an effective complex parameter b_0 corresponding to attraction, greatly improved fits are obtained with a density-dependent potential, where the fixed b_0 is replaced by

$$b_0 + B_0[\rho(r)/\rho_0]^\alpha, \quad (11)$$

with b_0, B_0 and $\alpha \geq 0$ determined by fits to the data. Fitted potentials of this kind are marked DD. This parameterization offers the advantage of fixing b_0 at its (repulsive) free-space value in order to respect the low-density limit, while relegating the expected in-medium attraction to the B_0 term which goes with a higher power of the density.

The departure of the optical potential from the fixed- t $t\rho$ approach was recently given a more intrinsically geometrical meaning within a model [11] where, loosely speaking, V_{opt} follows the shape of a function $F(r)$ inside, and the shape of $[1 - F(r)]$ outside the nucleus:

$$b_0 \rightarrow B_0 F(r) + b_0 [1 - F(r)], \quad F(r) = \frac{1}{e^x + 1}, \quad (12)$$

with $x = (r - R_x)/a_x$. Then clearly $F(r) \rightarrow 1$ for $(R_x - r) \gg a_x$, which defines the internal region. Likewise $[1 - F(r)] \rightarrow 1$ for $(r - R_x) \gg a_x$, which defines the external region. Thus R_x forms an approximate border between the internal and the external regions, and if R_x is close to the radius of the nucleus and a_x is of the order of 0.5 fm, then the two regions will correspond to the high density and low density regions of nuclear matter, respectively. This is indeed the case, as found in global fits to kaonic atom data [11]. The parameter b_0 represents the low-density interaction and the parameter B_0 represents the interaction inside the nucleus. We note that, unlike with pionic and antiprotonic atoms, the dependence of kaonic atom fits on the rms radius of the neutron distribution is weak, and the explicit inclusion of isovector terms, such as b_1 of Eq. (2), has only marginal effect.

Figure 2 (left) shows, as an example, the real part of the best-fit potential for ^{58}Ni obtained with the various models discussed above, i.e. the simple $t\rho$ model and its DD extension, and the geometrical model F, with the corresponding values of χ^2 for 65 data points in parentheses. Also shown, with an error band, is a Fourier-Bessel (FB) fit [7] that is discussed below. We note that, although the two density-dependent potentials marked DD and F have very different parameterizations, the resulting potentials are quite similar. In particular, the shape of potential F departs appreciably from $\rho(r)$ for $\rho(r)/\rho_0 \leq 0.2$, where the physics of the $\Lambda(1405)$ is expected to play a role. The density dependence of the potential F provides by far the best fit ever reported for any global K^- -atom data fit, and the lowest χ^2 value as reached by the model-independent FB method. On the right-hand side of the figure are shown the individual contributions to χ^2 of the shifts for the deep F potential and the shallow chirally-based potential (of depth about 50 MeV) due to Baca et al. [12]. It is self evident that the agreement between calculation and experiment is substantially better for the deep F potential than for the shallow chiral potential.

The question of how well the real part of the K^- -nucleus potential is determined was discussed in Ref. [7]. Estimating the uncertainties of hadron-nucleus potentials as function of position is not a simple task. For example, in the ‘ $t\rho$ ’ approach the shape of the potential is determined by the nuclear density distribution and the uncertainty in the strength parameter, as obtained from χ^2 fits to the data, implies a fixed *relative* uncertainty at all radii, which is, of course, unfounded. Details vary when more elaborate forms such as DD or F are

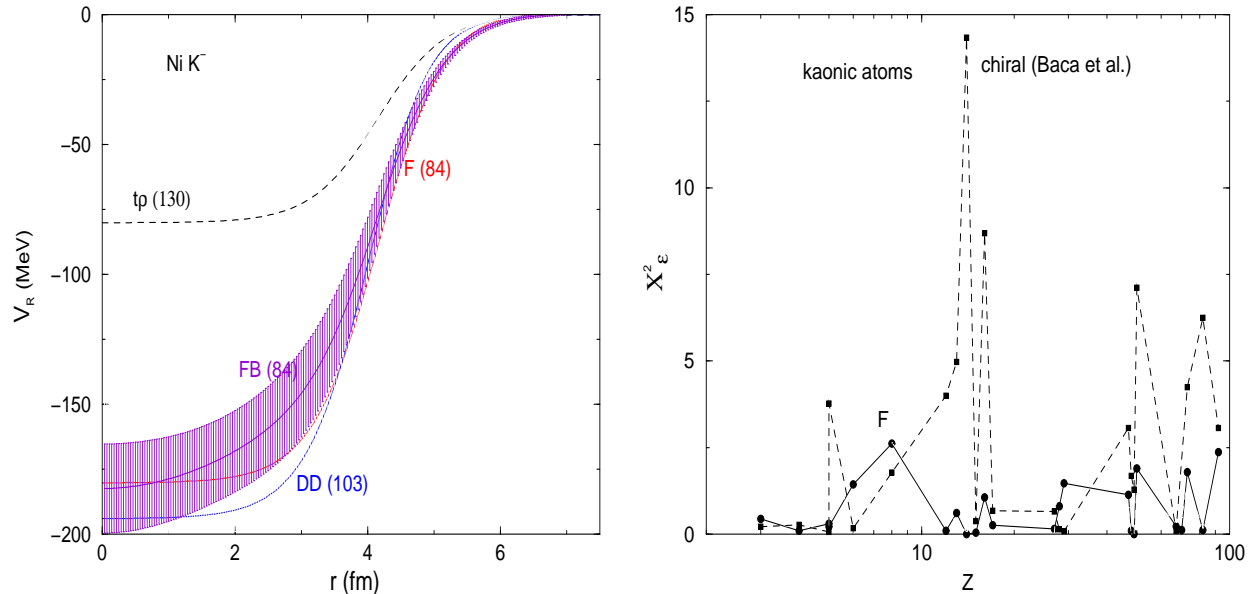


FIG. 2: Left: real part of the $\bar{K}^{-58}\text{Ni}$ potential obtained in a global fit to K^{-} -atom data using the model-independent FB technique [7], in comparison with other best-fit potentials and χ^2 values in parentheses. Right: contributions to the χ^2 of K^{-} atomic shifts for the *deep* density-dependent potential F from Ref. [11] and for the *shallow* chiral-based potential from Ref. [12].

used, but one is left essentially with *analytical continuation* into the nuclear interior of potentials that might be well-determined only close to the nuclear surface. ‘Model-independent’ methods have been used in analyses of elastic scattering data for various projectiles [13] to alleviate this problem. However, applying e.g. the Fourier-Bessel (FB) method in global analyses of kaonic atom data, one ends up with too few terms in the series, thus making the uncertainties unrealistic in their dependence on position. This is illustrated in Fig. 2 by the FB curve, obtained by adding a Fourier-Bessel series to a $t\rho$ potential. Only three terms in the series are needed to achieve a χ^2 of 84 and the potential becomes deep, in agreement with the other two ‘deep’ solutions. The error band obtained from the FB method [13] is, nevertheless, unrealistic because only three FB terms are used. However, an increase in the number of terms is found to be unjustified numerically.

The functional derivative (FD) method for identifying the radial regions to which exotic atom data are sensitive was described in detail in Sect. II C. This method was applied in Ref. [7] to the F and $t\rho$ kaonic atom potentials and results are shown in Fig. 3 where η is a global parameter defined by $r = R_c + \eta a_c$, with R_c and a_c the radius and diffuseness parameters, respectively, of a 2pF charge distribution. From the figure it can be inferred that the sensitive region for the real $t\rho$ potential is between $\eta = -1.5$ and $\eta = 6$ whereas for the F potential it is between $\eta = -3.5$ and $\eta = 4$. Recall that $\eta = -2.2$ corresponds to 90% of the central charge density and $\eta = 2.2$ corresponds to 10% of that density. It therefore becomes clear that within the $t\rho$ potential there is no sensitivity to the interior of the nucleus whereas with the density-dependent F potential, which yields greatly improved fit to the data, there is sensitivity to regions within the full nuclear density. The different sensitivities result from the potentials themselves: for the $t\rho$ potential the interior of the nucleus is masked essentially by the strength of the imaginary potential. In contrast, for

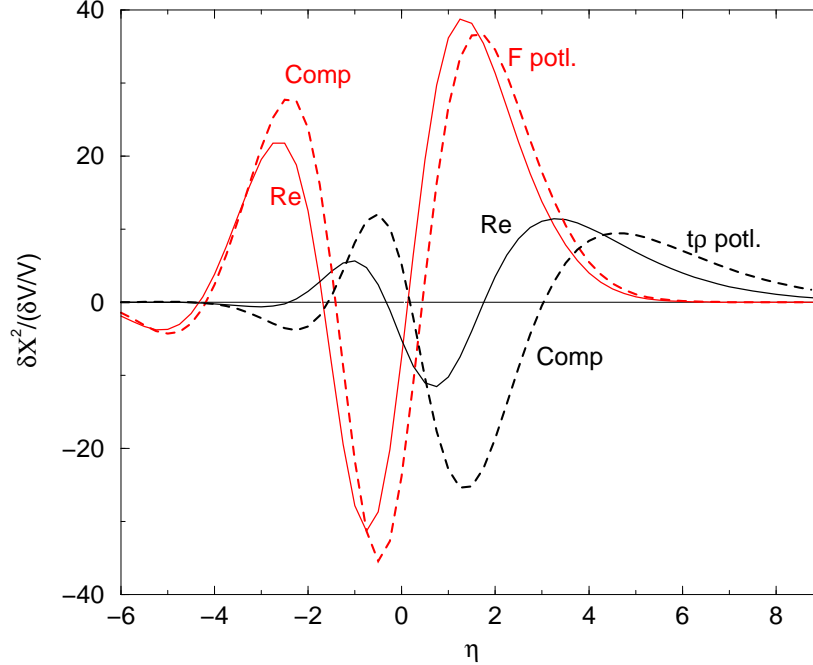


FIG. 3: Functional derivatives of kaonic atoms χ^2 with respect to the fully complex (Comp, dashed lines) and real (Re, solid lines) potential as function of η , where $r = R_c + \eta a_c$, with R_c and a_c the radius and diffuseness parameters, respectively, of a 2pF charge distribution. Results are shown for the tp and for the F potentials of Ref. [11] obtained from global fits to kaonic atom data.

the F potential not only is its imaginary part significantly smaller than the imaginary part of the tp potential [11] but also the additional attraction provided by the deeper potential enhances the *atomic* wavefunctions within the nucleus [1] thus creating the sensitivity at smaller radii. As seen in the figure, the functional derivative for the complex F potential is well approximated by that for its real part.

The optical potentials derived from the observed strong-interaction effects in kaonic atoms are sufficiently deep to support deeply-bound antikaon *nuclear* states, but it does not necessarily imply that such states are sufficiently narrow to be resolved unambiguously from experimental spectra. Moreover, choosing between the very shallow chirally motivated potentials [14, 15], the intermediate chiral potentials of depth around 100 MeV [16] or the deep phenomenological potentials of type F adds appreciable ambiguity to predictions made for such states. It should also be kept in mind that these depths relate to \bar{K} potentials at *threshold*, whereas the information required for \bar{K} -nuclear quasibound states is at energies of order 100 MeV below threshold. Predictions become model independent only when it comes to ‘deeply-bound’ K^- *atomic* states, as discussed below.

B. Deeply bound K^- atomic states

Somewhat paradoxically, due to the strong absorptive imaginary part of the K^- -nucleus potential, relatively narrow deeply-bound atomic states are expected to exist which are quite independent of the real potential. Such states are indeed found in numerical calculations as demonstrated in Fig. 4 where calculated binding energies and widths of atomic states of K^-

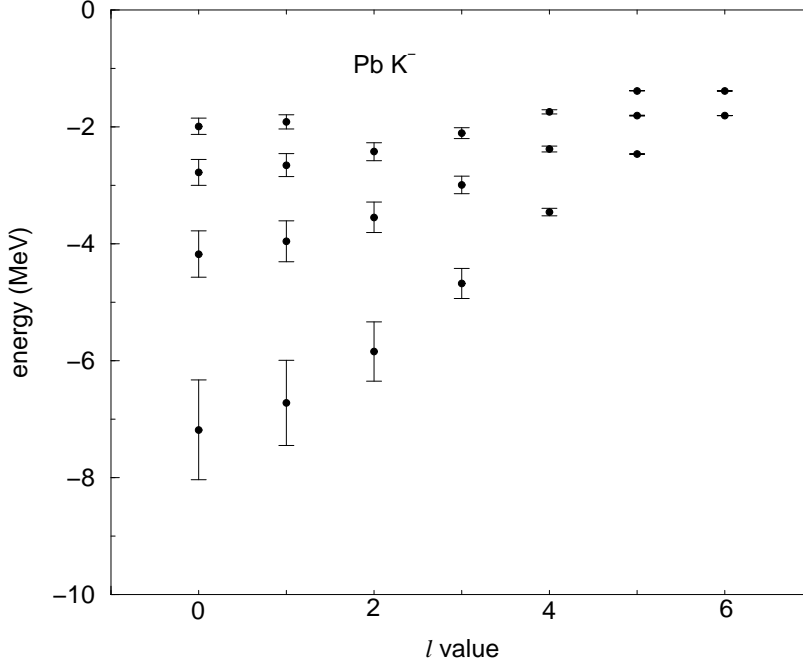


FIG. 4: Calculated energies of K^- atomic states in ^{208}Pb . The lowest energy for each l value corresponds to $n = l + 1$. The bars represent the widths of the states.

in ^{208}Pb are shown for several l -values, down to states which are inaccessible via the X-ray cascade. For ^{208}Pb , the last observed atomic circular state is the $7i$, corresponding to $l = 6$. The general physics behind this phenomenon is similar to that responsible for the deeply-bound pionic atom states, although there are differences in the underlying mechanisms. The mechanism behind the pionic atom deeply bound states is simply the *repulsive* real part of the s -wave potential which expels the atomic wavefunction ψ_{atom} from the nucleus, thus reducing the overlap between ψ_{atom} and the imaginary potential. This reduction, according to

$$\Gamma = -2 \frac{\int |\psi_{\text{atom}}|^2 \text{Im} V_{\text{opt}} d\mathbf{r}}{\int |\psi_{\text{atom}}|^2 d\mathbf{r}}, \quad (13)$$

results in a reduced width for atomic states. Eq. (13) holds *exactly* for a Schrödinger equation, with only small changes for a KG equation, see Refs. [17, 18]. In contrast, phenomenological kaonic atom potentials are *attractive*, but the strengths of the imaginary potential are such that the decay of ψ_{atom} as it enters the nucleus is equivalent to repulsion, resulting in narrow atomic states due to the reduced overlap as discussed above. It is seen from Fig. 4 that there is a saturation phenomenon where widths hardly increase for $l \leq 2$, contrary to intuitive expectation. The repulsive effect of sufficiently strong absorption is responsible for the general property of saturation of widths of atomic states and also for saturation of reaction cross sections above threshold, observed experimentally for antiprotons [19].

The left-hand side of Fig. 5 shows the saturation of widths as function of the absorptive strength parameter $\text{Im } b_0$ of V_{opt} , Eq. (2), for the $2p$ state of kaonic atoms of ^{208}Pb . For small values of $\text{Im } b_0$ the calculated width increases linearly, but already at 20% of the best-fit value of 0.9 fm saturation sets in and eventually the width goes down with further increase of the absorption. Note that the real part of the binding energy, represented here by the

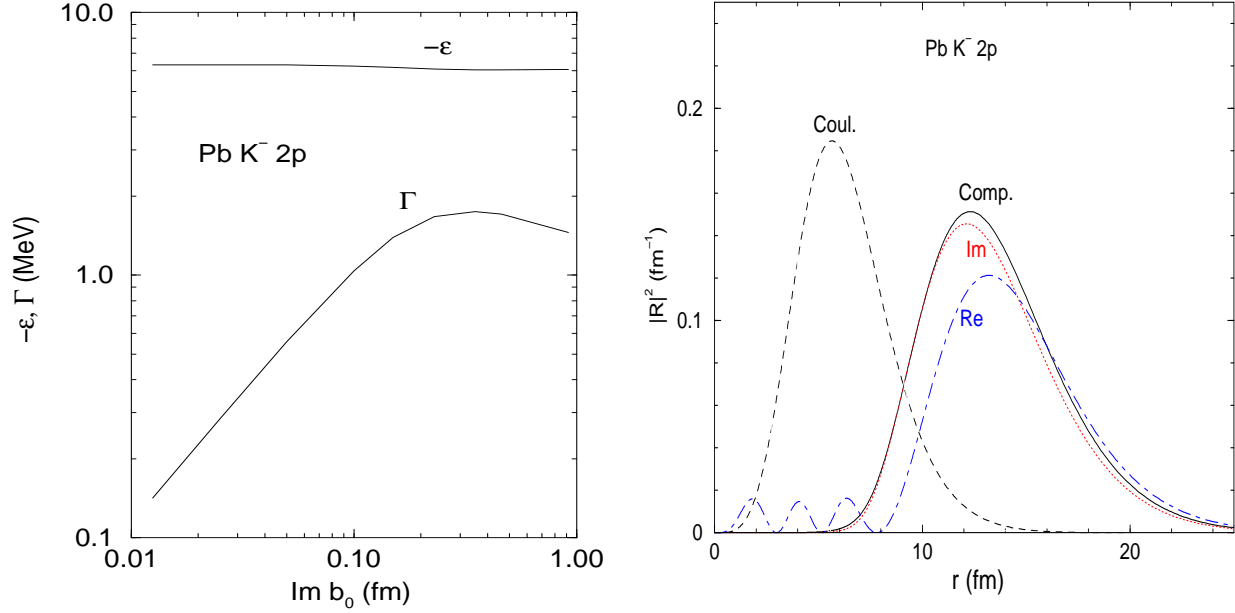


FIG. 5: Left: saturation of width Γ for the $2p$ ‘deeply bound’ K^- atomic state in ^{208}Pb as function of absorptivity $\text{Im } b_0$, for $\text{Re } b_0 = 0.62$ fm. Right: wavefunctions for this state, see text.

strong-interaction level shift ϵ , hardly changes with $\text{Im } b_0$. The right-hand side of Fig. 5 shows radial wavefunctions for the $2p$ atomic K^- state in ^{208}Pb for several combinations of potentials. The dashed curve marked ‘Coul’ is for the Coulomb potential only, and with a half-density radius for ^{208}Pb of 6.7 fm it clearly overlaps strongly with the nucleus. Adding the full complex optical potential the solid curve marked ‘Comp’ shows that the atomic wavefunction is expelled from the nucleus, and the dotted curve marked ‘Im’ shows that this repulsion is effected by the imaginary part of the potential. Clearly the overlap of the atomic wavefunction with the nucleus is dramatically reduced compared to the Coulomb-only situation. An interesting phenomenon is displayed by the dot-dashed curve marked ‘Re’. It shows the atomic wavefunction when the real potential is added to the Coulomb potential, demonstrating significant *repulsion* of the atomic wavefunction by the added *attractive* potential. The explanation for this bizarre result is provided by the three small peaks inside the nucleus which are due to the orthogonality of the *atomic* wavefunction and strongly-bound K^- *nuclear* wavefunctions having the same l -values. This extra structure of the atomic wavefunction in the interior effectively disappears when the imaginary potential is included.

IV. \bar{K} NUCLEAR INTERACTIONS

A. The K^-p interaction near threshold

The K^-p data at low energies provide a good experimental base upon which models for the strong interactions of the $\bar{K}N$ system have been developed. Near threshold the coupling to the open $\pi\Sigma$ and $\pi\Lambda$ channels is extremely important, as may be judged from the size of the K^-p reaction cross sections, particularly $K^-p \rightarrow \pi^+\Sigma^-$, with respect to the K^-p elastic cross sections shown in Fig. 6. By developing potential models, $\bar{K}N$ amplitudes are obtained

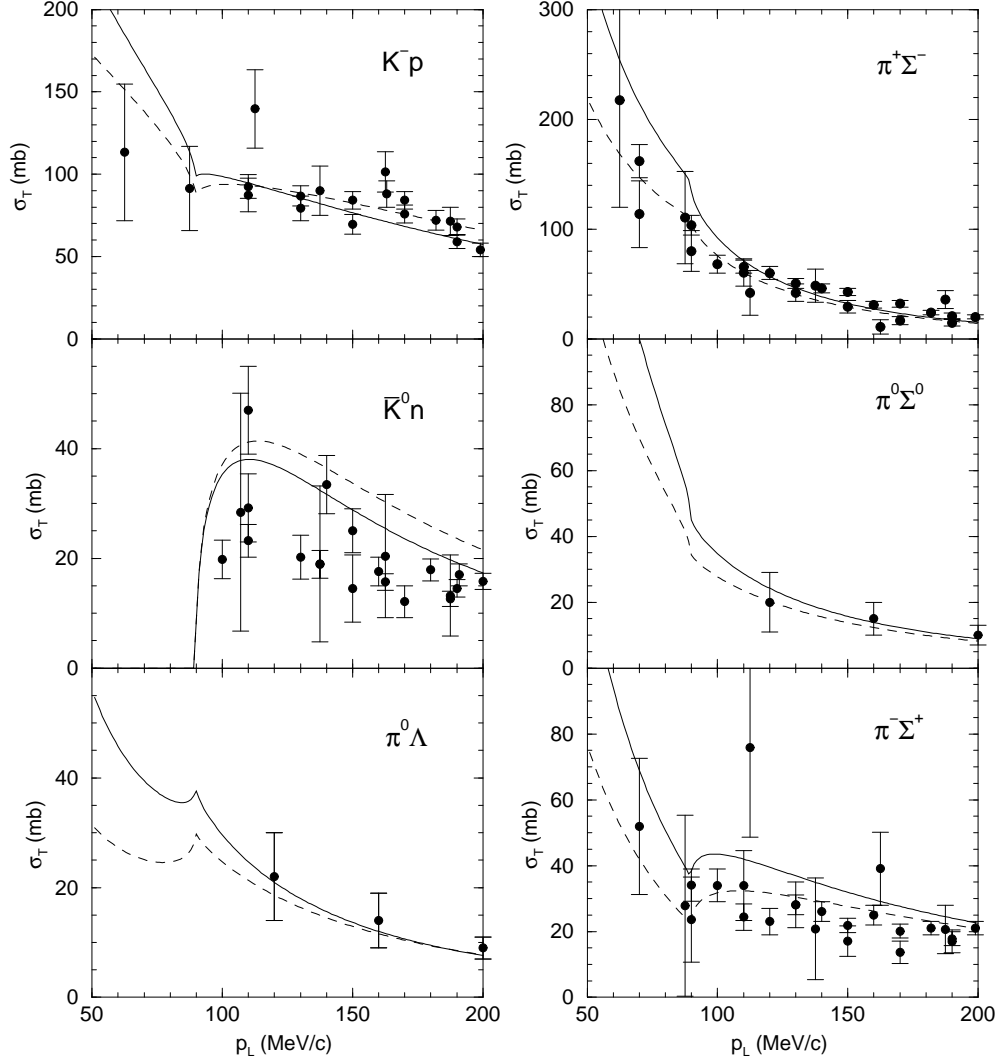


FIG. 6: Calculations from Ref. [15] of cross sections for K^-p scattering and reactions. The dashed lines show free-space chiral-model coupled-channel calculations. The solid lines show chiral-model coupled-channel calculations using slightly varied parameters in order to fit also the K^- -atom data for a (shallow) optical potential calculated self consistently.

that allow for analytic continuation into the nonphysical region below K^-p threshold. Using a K-matrix analysis, this was the way Dalitz and Tuan predicted the existence of the $\Lambda(1405)$ $\pi\Sigma$, $I = 0$ resonance in 1959 [20].

A recent example from coupled-channel potential model calculations [21, 22, 23, 24], based on low-energy chiral expansion of meson-baryon potentials in the $S = -1$ sector, is shown in Fig. 7 where the real and imaginary parts of the resulting K^-p elastic scattering amplitude, continued analytically below the K^-p threshold, are plotted. The line marked WT stands for the leading Weinberg-Tomozawa (WT) nonresonant K^-p amplitude below threshold when channel-coupling effects are switched off. The figure demonstrates that the $\Lambda(1405)$ resonance is generated *dynamically* within the coupled-channel calculation. A discrepancy with $\text{Im } a_{K^-p}$ deduced from the DEAR measurement [25] is highlighted in this figure. In contrast, the purely $I = 1$ K^-n amplitude does not show such resonance effects

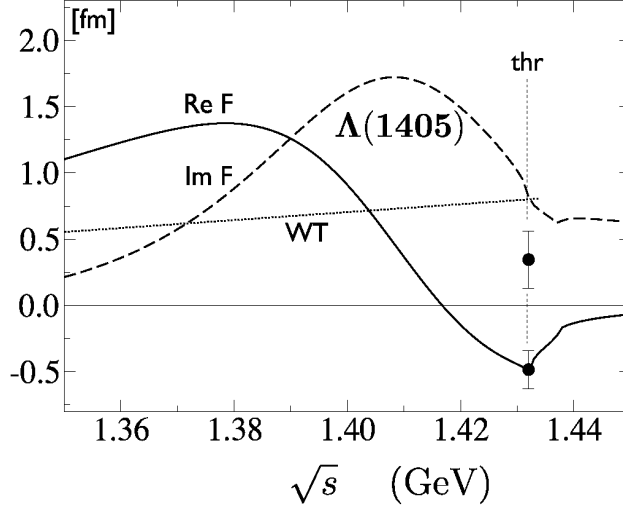


FIG. 7: Real and imaginary parts of the K^-p forward elastic scattering amplitude, fitted within a NLO chiral SU(3) coupled-channel approach to K^-p scattering and reaction data. The line denoted WT is the (real) LO Tomozawa-Weinberg K^-p driving-term amplitude. The DEAR measurement [25] value for a_{K^-p} is shown with error bars. Figure taken from Ref. [26], based on the work of Ref. [22].

below threshold, and its chiral model dependence is considerably weaker than the model dependence of amplitudes affected by the $\Lambda(1405)$ resonance, e.g. the K^-p elastic scattering amplitude shown in Fig. 7.

B. \bar{K} -nucleus potentials

The gross features of low-energy $\bar{K}N$ physics, as demonstrated in the previous section by chiral coupled-channel fits to the low-energy K^-p scattering and reaction data, are encapsulated in the lowest-order (LO) WT vector term of the chiral effective Lagrangian [27]. The Born approximation for the \bar{K} -nuclear optical potential $V_{\bar{K}}$ due to the driving-term WT interaction yields then a sizable attraction:

$$V_{\bar{K}} = -\frac{3}{8f_\pi^2} \rho \sim -55 \frac{\rho}{\rho_0} \text{ MeV} \quad (14)$$

for $\rho_0 = 0.16 \text{ fm}^{-3}$, where $f_\pi \sim 93 \text{ MeV}$ is the pseudoscalar meson decay constant. Iterating the TW term plus next-to-leading-order (NLO) terms, within an *in-medium* coupled-channel approach constrained by the $\bar{K}N - \pi\Sigma - \pi\Lambda$ data near the $\bar{K}N$ threshold, roughly doubles this \bar{K} -nucleus attraction as may be seen by inspecting Fig. 7. It is found (e.g. Ref. [16]) that the $\Lambda(1405)$ quickly dissolves in the nuclear medium at low density, so that the repulsive free-space scattering length a_{K^-p} , as function of ρ , becomes *attractive* well below ρ_0 . Since the purely $I = 1$ attractive scattering length a_{K^-n} is only weakly density dependent, the resulting in-medium $\bar{K}N$ isoscalar scattering length $b_0(\rho) = \frac{1}{2}(a_{K^-p}(\rho) + a_{K^-n}(\rho))$ translates into a strongly attractive $V_{\bar{K}}$:

$$V_{\bar{K}}(r) = -\frac{2\pi}{\mu_{KN}} b_0(\rho) \rho(r), \quad \text{Re}V_{\bar{K}}(\rho_0) \sim -110 \text{ MeV}. \quad (15)$$

However, when $V_{\bar{K}}$ is calculated *self consistently*, including $V_{\bar{K}}$ in the propagator G_0 used in the Lippmann-Schwinger equation determining $b_0(\rho)$, one obtains $\text{Re}V_{\bar{K}}(\rho_0) \sim -(40\text{-}60)$ MeV [14, 15, 28, 29]. The main reason for this weakening of $V_{\bar{K}}$, approximately going back to that calculated using Eq. (14), is the strong absorptive effect which $V_{\bar{K}}$ exerts within G_0 to suppress the higher Born terms of the $\bar{K}N$ TW potential.

Additional considerations for estimating $V_{\bar{K}}$ are listed below.

- QCD sum-rule estimates [30] for vector (v) and scalar (s) self-energies:

$$\Sigma_v(\bar{K}) \sim -\frac{1}{2} \Sigma_v(N) \sim -\frac{1}{2} (200) \text{ MeV} = -100 \text{ MeV}, \quad (16)$$

$$\Sigma_s(\bar{K}) \sim \frac{m_s}{M_N} \Sigma_s(N) \sim \frac{1}{10} (-300) \text{ MeV} = -30 \text{ MeV}, \quad (17)$$

where m_s is the strange-quark (current) mass. The factor 1/2 in Eq. (16) is due to the one nonstrange antiquark \bar{q} in the \bar{K} meson out of two possible, and the minus sign is due to G-parity going from q to \bar{q} . This rough estimate gives then $V_{\bar{K}}(\rho_0) \sim -130$ MeV.

- The QCD sum-rule approach essentially refines the mean-field argument [31, 32]

$$V_{\bar{K}}(\rho_0) \sim \frac{1}{3} (\Sigma_s(N) - \Sigma_v(N)) \sim -170 \text{ MeV}, \quad (18)$$

where the factor 1/3 is again due to the one nonstrange antiquark in the \bar{K} meson, but here with respect to the three nonstrange quarks of the nucleon.

- The ratio of K^-/K^+ production cross sections in nucleus-nucleus and proton-nucleus collisions near threshold, measured by the Kaon Spectrometer (KaoS) collaboration [33] at SIS, GSI, yields an estimate $V_{\bar{K}}(\rho_0) \sim -80$ MeV by relying on BUU transport calculations normalized to the value $V_K(\rho_0) \sim +25$ MeV. Since $\bar{K}NN \rightarrow YN$ absorption processes apparently were disregarded in these calculations, a deeper $V_{\bar{K}}$ may follow once nonmesonic absorption processes are included.

C. Deeply bound K^- nuclear states in light nuclei

The first prediction of a \bar{K} -nuclear quasibound state was made by Nogami [34] as early as 1963, arguing that the $I = 1/2$, $L = S = 0$ state of the K^-pp system could be bound by about 10 MeV. Recent calculations confirm this prediction, with higher values of binding energies but also with substantial values for the (mesonic) width of this state, as summarized in Table I. We note that the Faddeev calculations listed in the table account rigorously for the strong $I = 0$ $\bar{K}N \rightarrow \Sigma N$ coupling, but all the calculations overlook the $\bar{K}NN \rightarrow YN$ coupling to nonmesonic channels which are estimated to add conservatively 20 MeV to the overall width. If K^-pp , the lightest possible \bar{K} -nuclear system, is indeed bound, then it is plausible that heavier \bar{K} -nuclear systems will also possess quasibound states and the remaining question is whether these states are sufficiently narrow to allow observation and identification. Unlike the saturation of width in K^- atoms, discussed in Sect. IIIB, no saturation mechanism holds for the width of \bar{K} -nuclear states which retain very good overlap with the potential.

TABLE I: Binding energies (B) and widths (Γ) calculated for K^-pp (in MeV).

channels	single channel		coupled channels	
Ref.	ATMS [35]	AMD [36]	Faddeev [37, 38]	Faddeev [39, 40]
B	48	20–50	50–70	60–95
Γ	61	–	90–110	45–80

Ongoing experiments by the FINUDA spectrometer collaboration at DAΦNE, Frascati, already claimed evidence for a relatively broad K^-pp deeply bound state ($B \sim 115$ MeV) by observing back-to-back Λp pairs from the decay $K^-pp \rightarrow \Lambda p$ in K^-_{stop} reactions on Li and ^{12}C [41], but these pairs could naturally arise from conventional absorption processes at rest when final-state interaction is taken into account [42]. Indeed, the $K^-_{\text{stop}}pn \rightarrow \Sigma^-p$ reaction observed recently in ^6Li [43] does not require any K^-d quasibound state. It is worth noting, however, that in order to search for a K^-pn bound state which is charge symmetric to the K^-pp quasibound state discussed above, one should use a ^7Li target to look for back-to-back Σ^-p pairs. Very recently, a Λp narrow peak has been reported in \bar{p} annihilation on ^4He from the OBELIX spectrometer data at LEAR, CERN [44], corresponding to a yet deeper K^-pp quasibound state ($B \sim 160$ MeV) if this interpretation is valid, given the reservations mentioned above. A definitive study of the K^-pp quasibound state (or more generally $\{\bar{K}[NN]_{I=1}\}_{I=1/2}$) could be reached through fully exclusive formation reactions, such as:

$$K^- + {}^3\text{He} \rightarrow n + \{\bar{K}[NN]_{I=1}\}_{I=1/2, I_z=+1/2}, \quad p + \{\bar{K}[NN]_{I=1}\}_{I=1/2, I_z=-1/2}, \quad (19)$$

the first of which is scheduled for day-one experiment in J-PARC [45]. We note that the large widths calculated for the K^-pp quasibound state could make it difficult to identify the state experimentally [46].

The current experimental and theoretical interest in \bar{K} -nuclear bound states was triggered back in 1999 by the suggestion of Kishimoto [47] to look for such states in (K^-, p) reactions in flight, and by Akaishi and Yamazaki [48, 49] who suggested to look for a $\bar{K}NNN$ $I = 0$ state bound by over 100 MeV for which the main $\bar{K}N \rightarrow \pi\Sigma$ decay channel would be kinematically closed. In fact, Wycech had conjectured that the width of such states could be as small as 20 MeV [50]. Evidence claimed initially for relatively narrow states in the inclusive (K^-_{stop}, p) and (K^-_{stop}, n) spectra on ^4He has recently been withdrawn [51, 52], just to be replaced by a complementary low-statistics Λd narrow peak reported in \bar{p} annihilation on ^4He [44], corresponding to a quasibound $\bar{K}NNN$ $I = 0$ state with $B \sim 120$ MeV. Such correlated Λd pairs could arise from secondary three-nucleon absorption processes, as recently discussed by the FINUDA [53] and the KEK [54] Collaborations in K^-_{stop} reactions on ^6Li and ^4He , respectively. On heavier targets, enhancements have been observed in the (K^-, n) in-flight spectrum on ^{16}O [55], but subsequent (K^-, n) and (K^-, p) reactions on ^{12}C at $p_{\text{lab}} = 1$ GeV/c have not disclosed any peaks beyond the appreciable strength observed below the \bar{K} -nucleus threshold [56]. It is clear that the issue of \bar{K} nuclear states is far yet from being experimentally resolved and more dedicated, systematic searches are necessary.

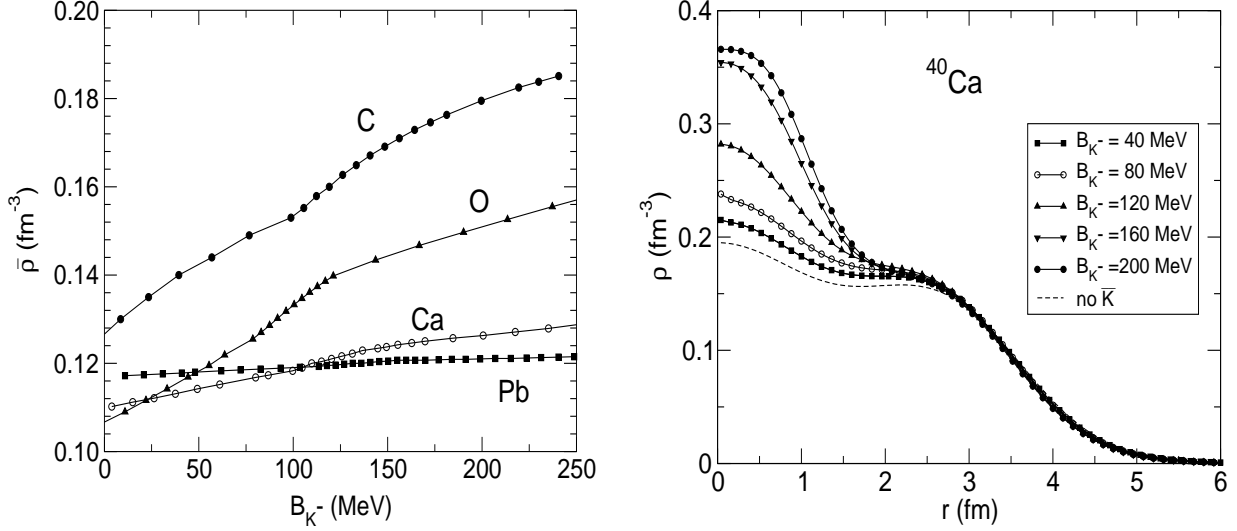


FIG. 8: Left: dynamically calculated average nuclear density $\bar{\rho}$ of $1s$ K^- -nuclear states in the nuclei denoted, as function of the $1s$ K^- binding energy. Right: dynamically calculated nuclear density ρ of ^{40}Ca for several $1s$ K^- nuclear states with specified B_{K^-} values [11].

D. RMF dynamical calculations of \bar{K} quasibound nuclear states

In this model, spelled out in Refs. [11, 57, 58], the (anti)kaon interaction with the nuclear medium is incorporated by adding to \mathcal{L}_N the Lagrangian density \mathcal{L}_K :

$$\mathcal{L}_K = \mathcal{D}_\mu^* \bar{K} \mathcal{D}^\mu K - m_K^2 \bar{K} K - g_{\sigma K} m_K \sigma \bar{K} K. \quad (20)$$

The covariant derivative $\mathcal{D}_\mu = \partial_\mu + ig_{\omega K} \omega_\mu$ describes the coupling of the (anti)kaon to the vector meson ω . The (anti)kaon coupling to the isovector ρ meson was found to have negligible effects. The \bar{K} meson induces additional source terms in the equations of motion for the meson fields σ and ω_0 . It thus affects the scalar $S = g_{\sigma N} \sigma$ and the vector $V = g_{\omega N} \omega_0$ potentials which enter the Dirac equation for nucleons, and this leads to rearrangement or polarization of the nuclear core, as shown on the left-hand side of Fig. 8 for the calculated average nuclear density $\bar{\rho} = \frac{1}{A} \int \rho^2 d\mathbf{r}$ as a function of B_{K^-} for K^- nuclear $1s$ states across the periodic table, and on the right-hand side of the figure for the density of ^{40}Ca for several $1s$ K^- nuclear states with specified B_{K^-} values [11]. It is seen that in the light K^- nuclei, $\bar{\rho}$ increases substantially with B_{K^-} to values about 50% higher than without the \bar{K} . The increase of the central nuclear densities is bigger, up to 50-100%, and is nonnegligible even in the heavier K^- nuclei where it is confined to a small region of order 1.5 fm. Furthermore, in the Klein-Gordon equation satisfied by the \bar{K} , the scalar $S = g_{\sigma K} \sigma$ and the vector $V = -g_{\omega K} \omega_0$ potentials become *state dependent* through the *dynamical* density dependence of the mean-field potentials S and V , as expected in a RMF calculation. An imaginary $\text{Im}V_{\bar{K}} \sim t\rho$ was added, fitted to the K^- atomic data [59]. It was then suppressed by an energy-dependent factor $f(B_{\bar{K}})$, considering the reduced phase-space for the initial decaying state and assuming two-body final-state kinematics for the decay products in the $\bar{K}N \rightarrow \pi Y$ mesonic modes (80%) and in the $\bar{K}NN \rightarrow YN$ nonmesonic modes (20%).

The RMF coupled equations were solved self-consistently. For a rough idea, whereas the static calculation gave $B_{K^-}^{1s} = 132$ MeV for the K^- $1s$ state in ^{12}C , using the values

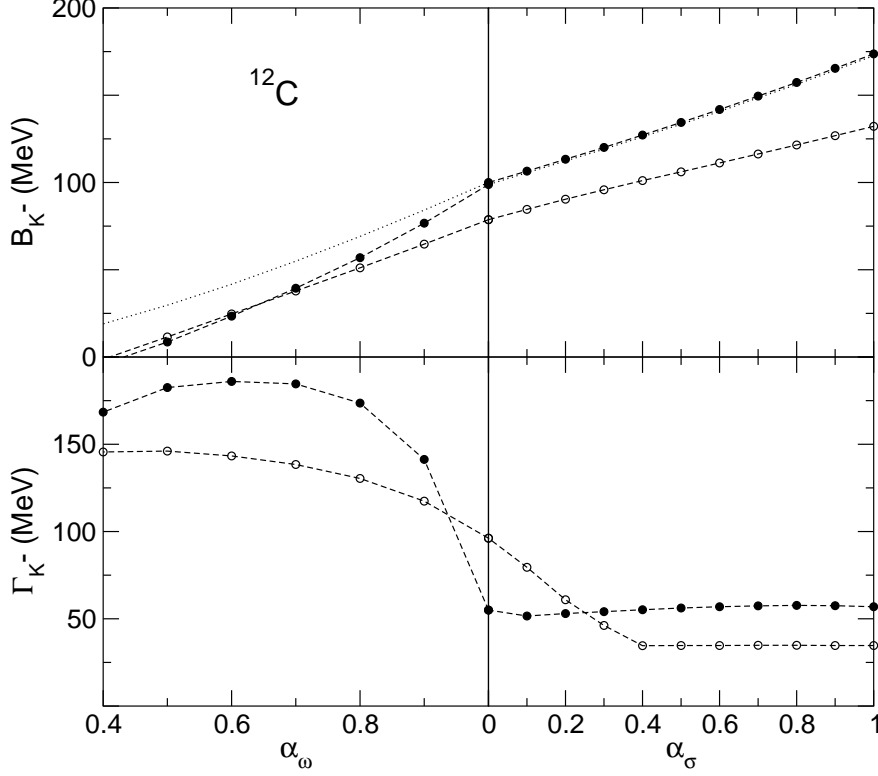


FIG. 9: $1s$ K^- binding energy and width in ^{12}C calculated statically (open circles) and dynamically (solid circles) for the nonlinear RMF model NL-SH [60] as function of the ωK and σK coupling strengths: α_ω is varied in the left panels as indicated, with $\alpha_\sigma = 0$, and α_σ is varied in the right panels as indicated, with $\alpha_\omega = 1$. The dotted line shows the calculated binding energy when the absorptive K^- potential is switched off in the dynamical calculation.

$g_{\omega K}^{\text{atom}}$, $g_{\sigma K}^{\text{atom}}$ from the K^- -atom fit, the dynamical calculation gave $B_{K^-}^{1s} = 172$ MeV. In order to scan a range of values for $B_{K^-}^{1s}$, the coupling constants $g_{\sigma K}$ and $g_{\omega K}$ were varied in given intervals of physical interest. An example is shown in Fig. 9.

Beginning approximately with ^{12}C , the following conclusions may be drawn:

- For given values of $g_{\sigma K}, g_{\omega K}$, the \bar{K} binding energy $B_{\bar{K}}$ saturates as function of A , except for a small increase due to the Coulomb energy (for K^-).
- The difference between the binding energies calculated dynamically and statically, $B_{\bar{K}}^{\text{dyn}} - B_{\bar{K}}^{\text{stat}}$, is substantial in light nuclei, increasing with $B_{\bar{K}}$ for a given value of A , as shown in the upper panels of Fig. 9, and decreasing monotonically with A for a given value of $B_{\bar{K}}$. It may be neglected only for very heavy nuclei. The same holds for the nuclear rearrangement energy $B_{\bar{K}}^{\text{s.p.}} - B_{\bar{K}}$ which is a fraction of $B_{\bar{K}}^{\text{dyn}} - B_{\bar{K}}^{\text{stat}}$.
- The functional dependence of the width $\Gamma_{K^-}(B_{K^-})$, shown for ^{12}C in the lower panels of Fig. 9 follows the shape of the suppression factor $f(B_{K^-})$ which falls off rapidly until $B_{K^-} \sim 100$ MeV, where the dominant $\bar{K}N \rightarrow \pi\Sigma$ gets switched off, and then stays rather flat in the range $B_{K^-} \sim 100\text{--}200$ MeV where the width is dominated by the $\bar{K}NN \rightarrow YN$ absorption modes. The widths calculated dynamically in this range are considerably larger than if calculated statically. Adding the residual width neglected

in this calculation, due to the $\bar{K}N \rightarrow \pi\Lambda$ secondary mesonic decay channel, and assigning these two-nucleon absorption modes a ρ^2 density dependence, a lower limit of $\Gamma_{\bar{K}} \gtrsim 50$ MeV is obtained for deeply-bound states in the range $B_{K^-} \sim 100$ -200 MeV [58].

E. Kaon condensation

The possibility of kaon condensation in dense matter was proposed by Kaplan and Nelson [61, 62], with subsequent works offering related scenarios in nuclear matter [63, 64]. Neutron stars, with a density range extending to several times nuclear-matter density, have been considered extensively as the most natural dense systems where kaon condensation is likely to be realized. It is commonly accepted that under some optimal conditions, kaon condensation could occur at densities above $3\rho_0$ depending on the way hyperons enter the constituency of neutron stars. However, our concern here is not with neutron stars where time scales of the weak interactions are operative, enabling the transformation $n \rightarrow p + K^-$ or a rare weak decay such as $e^- \rightarrow K^- + \nu_e$ to transform ‘high-energy’ electrons to antikaons once the effective mass of K^- mesons dropped below 200 MeV approximately. Our concern here is limited to laboratory strong-interaction processes where hadronization and equilibration time scales in collisions leading to dense matter are much shorter, of order fm/c. If antikaons bind strongly to nuclei, then one might ask whether or not the binding energy per \bar{K} meson in multi- \bar{K} nuclear states increases significantly upon adding a large number of \bar{K} mesons, so that \bar{K} mesons provide the physical degrees of freedom for self-bound strange hadronic systems. Precursor phenomena to kaon condensation in nuclear matter would occur beyond some threshold value of strangeness, if the binding energy $B_{\bar{K}}$ per \bar{K} meson exceeds the combination $m_K c^2 + \mu_N - m_\Sigma c^2 \gtrsim 240$ MeV, where μ_N is the nucleon chemical potential. Furthermore, once $B_{\bar{K}} \gtrsim m_K c^2 + \mu_N - m_\Lambda c^2 \gtrsim 320$ MeV, Λ , Σ and Ξ hyperons would no longer combine macroscopically with nucleons to compose the more conventional kaon-free form of strange hadronic matter [65].

Gazda et al. [58] recently calculated multi- \bar{K} nuclear configurations, finding that the nuclear and \bar{K} densities behave regularly upon increasing the number of antikaons embedded in the nuclear medium, without any indication for abrupt or substantial increase of the densities. The central nuclear densities appear to saturate at approximately 50% higher values than the central nuclear density with one antikaon, as shown on the left-hand side of Fig. 10 for multi- K^- ^{208}Pb nuclei. Furthermore, the \bar{K} binding energy saturates upon increasing the number of \bar{K} mesons embedded in the nuclear medium. The heavier the nucleus is, the more antikaons it takes to saturate the binding energies, but even for ^{208}Pb the number required does not exceed approximately 10, as shown on the right-hand side of Fig. 10. We note that the interaction between antikaons in this extended RMF calculation is mediated by isoscalar boson fields: vector ω and ϕ , and scalar σ . The binding-energy saturation owes its robustness to the dominance of the *repulsive* vector interactions over the attractive scalar interactions for antikaon pairs. The saturated values of \bar{K} binding energies do not exceed the range of values 100–200 MeV considered normally as providing deep binding for one antikaon. This range of binding energies leaves antikaons in multi- \bar{K} nuclei comfortably above the range of energies where hyperons might be relevant. It is therefore unlikely that multi- \bar{K} nuclei may offer precursor phenomena in nuclear matter towards kaon condensation.

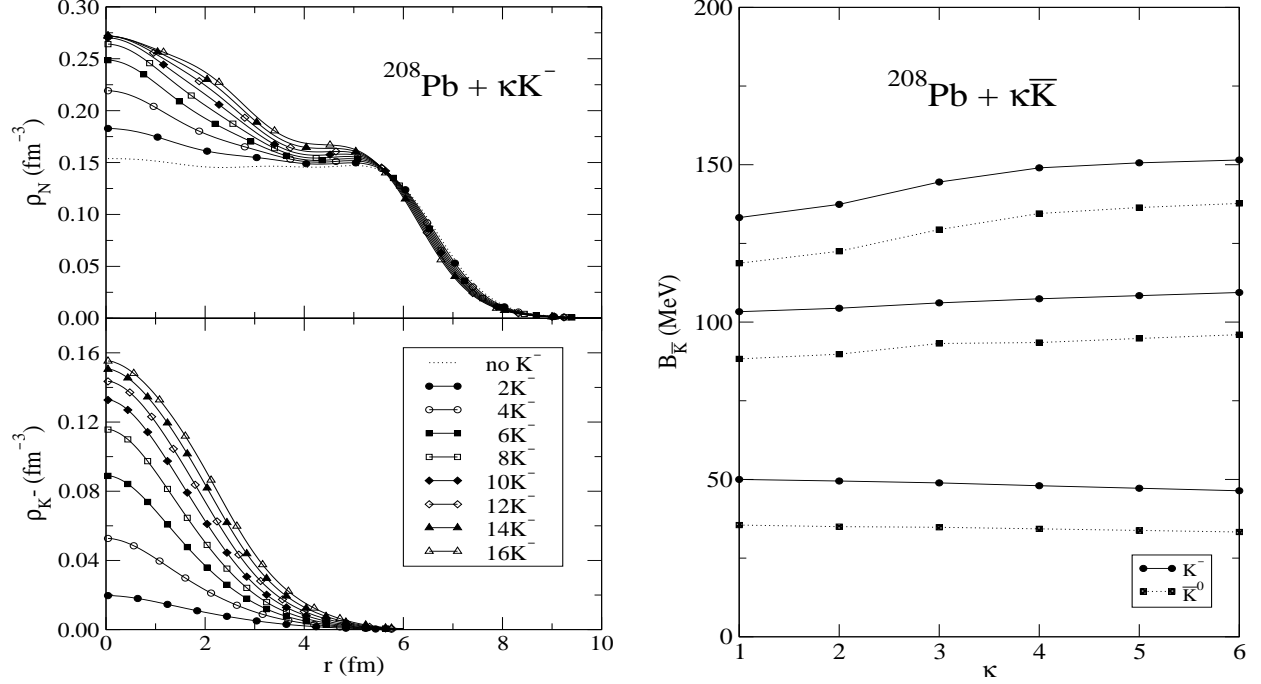


FIG. 10: Left: nuclear density ρ_N (top panel) and $1s \bar{K}$ density $\rho_{\bar{K}}$ (bottom panel) in $^{208}\text{Pb} + \kappa K^-$, starting with $B_{K^-} = 100$ MeV in $^{208}\text{Pb} + 1K^-$. The dotted curve stands for the ^{208}Pb density in the absence of \bar{K} mesons. Right: $1s \bar{K}$ binding energy $B_{\bar{K}}$ in $^{208}\text{Pb} + \kappa \bar{K}$, where $\bar{K} = K^-$ (circles) and \bar{K}^0 (squares). Figure taken from Ref. [58].

V. Σ HYPERONS

A. Overview

One Boson Exchange (OBE) models fitted to the scarce low-energy YN scattering data produce within a G -matrix approach, with one exception (Nijmegen Model F), as much attraction for the Σ nuclear potential as they do for the Λ nuclear potential, see Ref. [66] for a review of ‘old’ models and Ref. [67] for the latest state of the art for Nijmegen models. Indeed, the best-fit $t_{\text{eff}}\rho$ potential for Σ^- atoms was found by Batty et al. [68, 69] to be attractive and absorptive, with central depths for the real and imaginary parts of 25-30 MeV and 10-15 MeV, respectively. It took almost a full decade, searching for Σ hypernuclear bound states at CERN, KEK and BNL, before it was realized that except for a special case for $^4_\Sigma\text{He}$, the observed continuum Σ hypernuclear spectra indicate a very shallow, or even repulsive Σ nuclear potential, as reviewed by Dover et al. [70]. These indications have received firm support with the measurement of several (K^-, π^\pm) spectra at BNL [71] followed by calculations for ^9Be [72]. Recently, with measurements of the Σ^- spectrum in the (π^-, K^+) reaction taken at KEK across the periodic table [73, 74], it has become established that the Σ nuclear interaction is strongly repulsive. In parallel, analyses of Σ^- -atom in the early 1990s, allowing for density dependence or departure from the $t\rho$ prescription, motivated mostly by the precise data for W and Pb [75], led to the conclusion that the *nuclear* interaction of Σ s is dominated by repulsion [76, 77, 78], as reviewed in Ref. [1]. This might have interesting repercussions for the balance of strangeness in the inner crust of

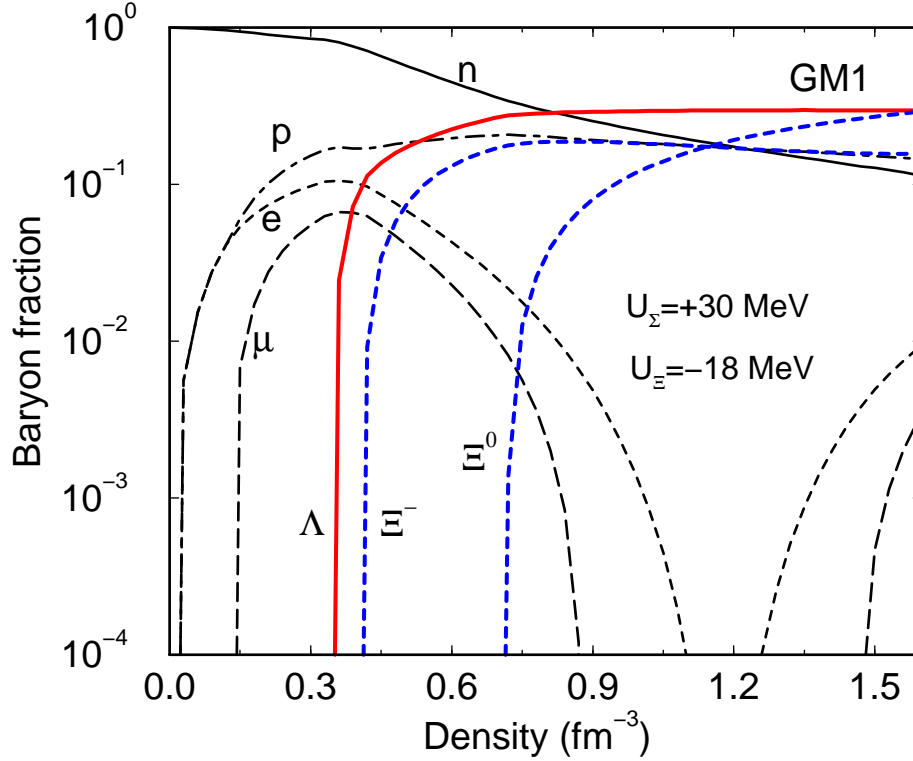


FIG. 11: Fractions of baryons and leptons in neutron-star matter for a RMF calculation using set GM1 with weak YY interactions [83]. Figure taken from Ref. [84].

neutron stars [79], primarily by delaying the appearance of Σ^- hyperons to higher densities, if at all, as discussed below. The inability of the Nijmegen OBE models, augmented by G-matrix calculations [67], to produce Σ nuclear repulsion is a serious drawback for these models at present. This problem apparently persists also in the Juelich model approach [80]. The only theoretical works that provide exception are SU(6) quark-model RGM calculations by the Kyoto-Niigata group [81], in which a strong Pauli repulsion appears in the $I = 3/2$, ${}^3S_1 - {}^3D_1$ ΣN channel, and Kaiser's SU(3) chiral perturbation calculation [82] which yields repulsion of order 60 MeV in nuclear matter.

Since Σ^- is the first hyperon (as function of density) to appear in neutron stars when the hyperon interactions are disregarded, it is natural to expect that the composition of neutron-star matter depends sensitively on the Σ^- -hypernuclear potential. For attractive Σ^- -hypernuclear potentials of the order of 30 MeV depth, as for Λ hyperons in Λ hypernuclei, the Σ^- is indeed the first hyperon to appear, at density lower than twice nuclear matter density. However, for a repulsive potential, the situation reverses dramatically as shown in Fig. 11. Incidentally, a K^- condensed phase might then appear at density between 3 to 4 times nuclear matter density replacing Ξ^- hyperons and second in strangeness only to Λ hyperons [85].

Below we briefly review and update the Σ^- atom fits and the recent (π^-, K^+) KEK results and their analysis.

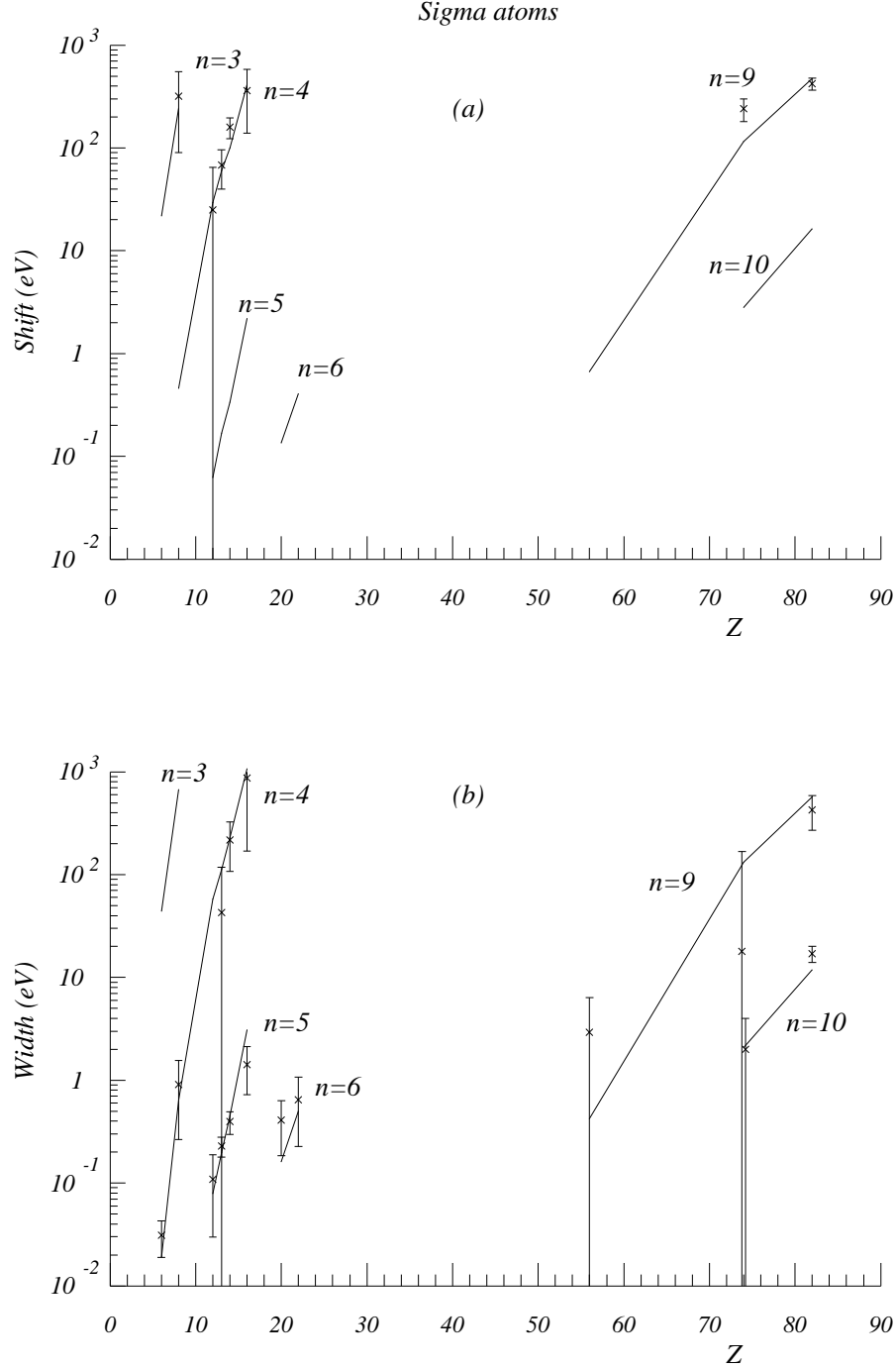


FIG. 12: Shift and width values for sigma atoms. The continuous lines join points calculated with a best-fit DD optical potential, see next figure.

B. Fits to Σ^- atoms

The data used in the Σ^- -atom fits are shown in Fig. 12 representing all published measurements from C to Pb inclusive. The data are relatively inaccurate, reflecting the difficulty in making measurements of strong-interaction effects in Σ^- atoms where most of the X-ray lines are relatively weak and must be resolved from the much stronger K^- atomic X-ray

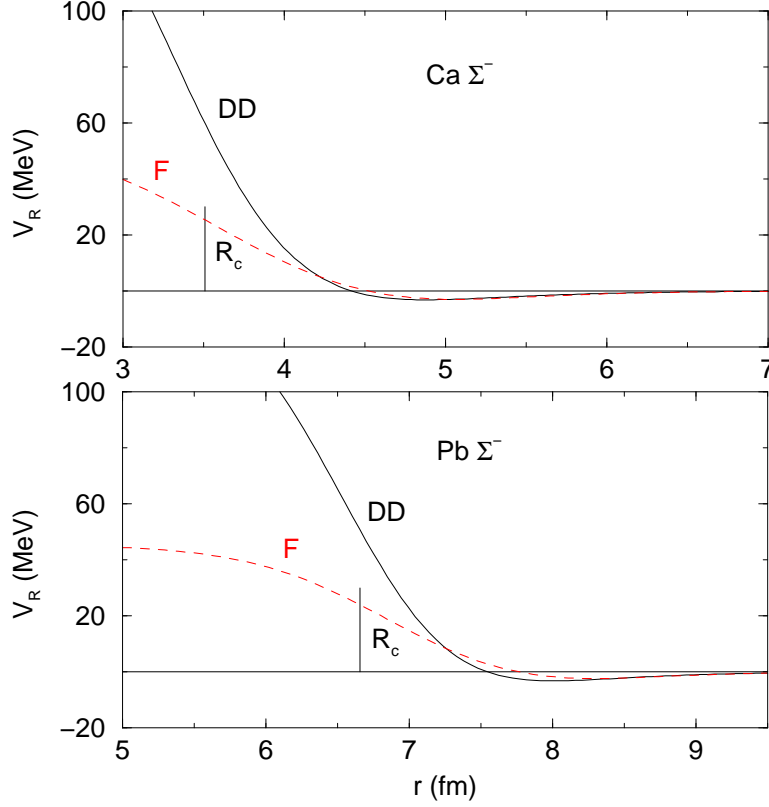


FIG. 13: $\text{Re}V_{\text{opt}}$ for DD (solid) and for the geometrical model F (dashed) Σ^- nuclear potentials fitted to Σ^- atomic data. Vertical bars indicate the half-density radius of the nuclear charge distribution.

transitions. Batty et al. [76, 77] analyzed the full data set of Σ^- atoms, consisting of strong-interaction level shifts, widths and yields, introducing a phenomenological density dependent (DD) potential of the isoscalar form

$$V_{\Sigma}(r) \sim [b_0 + B_0 (\rho(r)/\rho(0))^\alpha] \rho(r) \quad , \quad \alpha > 0 \quad , \quad (21)$$

and fitting the parameters b_0, B_0 and α to the data, greatly improved fits to the data are obtained. Isovector components are readily included in Eq. (21) but are found to have a marginal effect. Note, however, that the absorption was assumed to take place only on protons. The complex parameter b_0 may be identified with the spin-averaged $\Sigma^- N$ scattering length. For the best-fit isoscalar potentials, $\text{Re}V_{\Sigma}$ is attractive at low densities outside the nucleus, changing into repulsion in the nuclear surface region. The precise magnitude and shape of the repulsive component within the nucleus is not determined by the atomic data. The resulting potentials are shown in Fig. 13 (DD, solid lines), where it is worth noting that the transition from attraction to repulsion occurs well outside of the nuclear radius, hence the occurrence of this transition should be largely model independent. To check this last point we have repeated the fits to the atomic data with the ‘geometrical model’ F of Sect. III A, using separate $t\rho$ expressions in an internal and an external region, see Eq. (12). The neutron densities used in the fits were of the skin type, with the $r_n - r_p$ parameter Eq. (3) $\gamma=1.0$ fm. The fits deteriorate significantly if the halo type is used for the neutron density. The fit to the data is equally good with this model as with the DD model, (χ^2

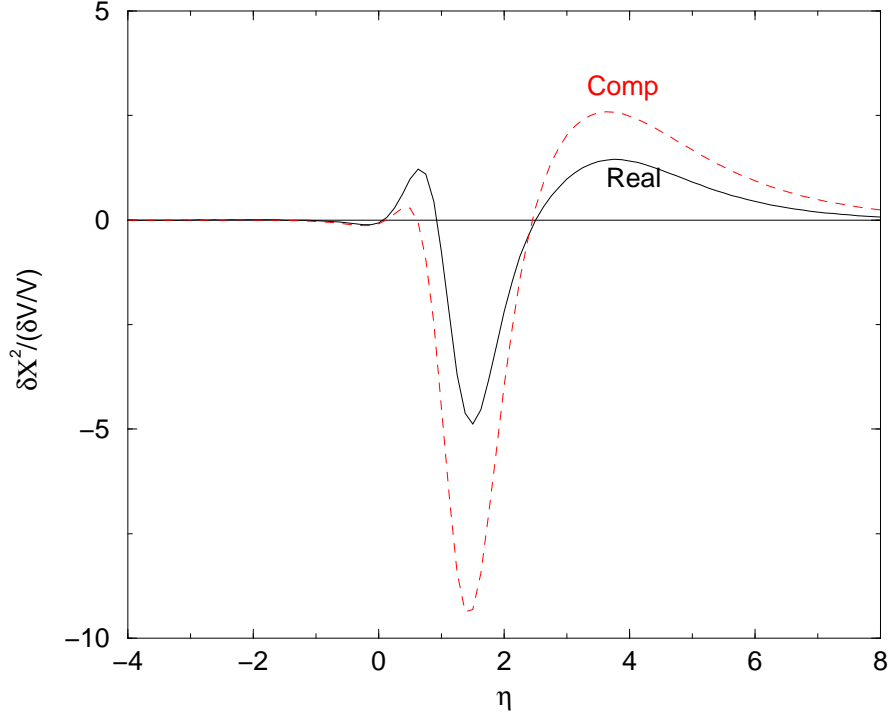


FIG. 14: Functional derivatives of χ^2 with respect to the real (solid) and with respect to the full complex (dashed) optical potentials for the best-fit F potential.

per degree of freedom of 0.9 here compared to 1.0 for the DD model) and the potentials are shown as the dashed lines in Fig. 13. The half-density radius of the charge distribution is indicated in the figure. It is clear that both models show weak attraction at large radii, turning into repulsion approximately one fm outside of that radius.

Further insight into the geometry of the Σ -nucleus interaction is gained by inspecting the functional derivatives (FD) of χ^2 with respect to the optical potentials, see Sect. II C. Figure 14 shows the FDs based on the best fit of the geometrical model F as discussed above. From the differences between the FD with respect to the full complex potential and the FD with respect to the real potential it is concluded that both real and imaginary parts play similar roles in the Σ -nucleus interaction. The bulk of $|\text{FD}|$ is in the range of $0.5 \leq \eta \leq 6$, covering the radial region where the weak attraction turns into repulsion. Obviously no information is obtained from Σ^- atoms on the interaction inside the nucleus. It is also interesting to note quite generally that such potentials do not produce bound states, and this conclusion is in agreement with the experimental results from BNL [71] for the absence of Σ hypernuclear peaks beyond He.

Some semi-theoretical support for this finding of inner repulsion is given by RMF calculations by Mareš et al. [78] who generated the Σ -nucleus interaction potential in terms of scalar (σ) and vector (ω, ρ) meson mean field contributions, fitting its coupling constants to the relatively accurate Σ^- atom shift and width data in Si and in Pb. The obtained potential fits very well the whole body of data on Σ^- atoms. This potential, which is generally attractive far outside the nucleus, becomes repulsive at the nuclear surface and remains so inward in most of the acceptable fits, of order 10-20 MeV. The Pb data [75] are particularly important in pinning down the isovector component of the potential which in this model is sizable and

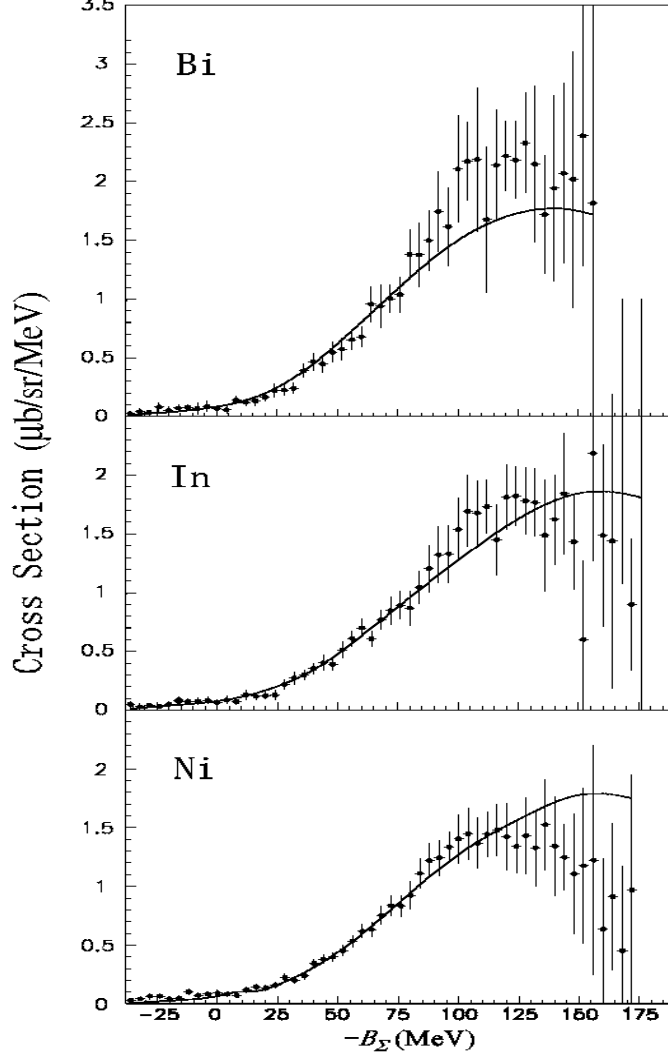


FIG. 15: Inclusive (π^-, K^+) spectra on Ni, In and Bi, fitted by a Σ -nucleus WS potential with depths $V_0 = 90$ MeV, $W_0 = -40$ MeV [74].

which, for Σ^- , acts against nuclear binding in core nuclei with $N - Z > 0$, countering the attractive Coulomb interaction. On the other hand, for very light nuclear cores and perhaps only for $A = 4$ hypernuclei, this isovector component (Lane term) generates binding of Σ^+ configurations. In summary, the more modern fits to Σ^- atom data [76, 77, 78] and the present fits with the geometrical model support the presence of a substantial repulsive component in the Σ -nucleus potential which excludes normal Σ -nuclear binding, except perhaps in very special cases such as ${}^4_\Sigma\text{He}$ [86, 87, 88, 89].

C. Evidence from (π^-, K^+) spectra

A more straightforward information on the nature of the Σ -nuclear interaction has been provided by recent measurements of inclusive (π^-, K^+) spectra on medium to heavy nuclear targets at KEK [73, 74]. The inclusive (π^-, K^+) spectra on Ni, In and Bi are shown in Fig. 15 together with a fit using Woods-Saxon potentials with depths $V_0 = 90$ MeV for the

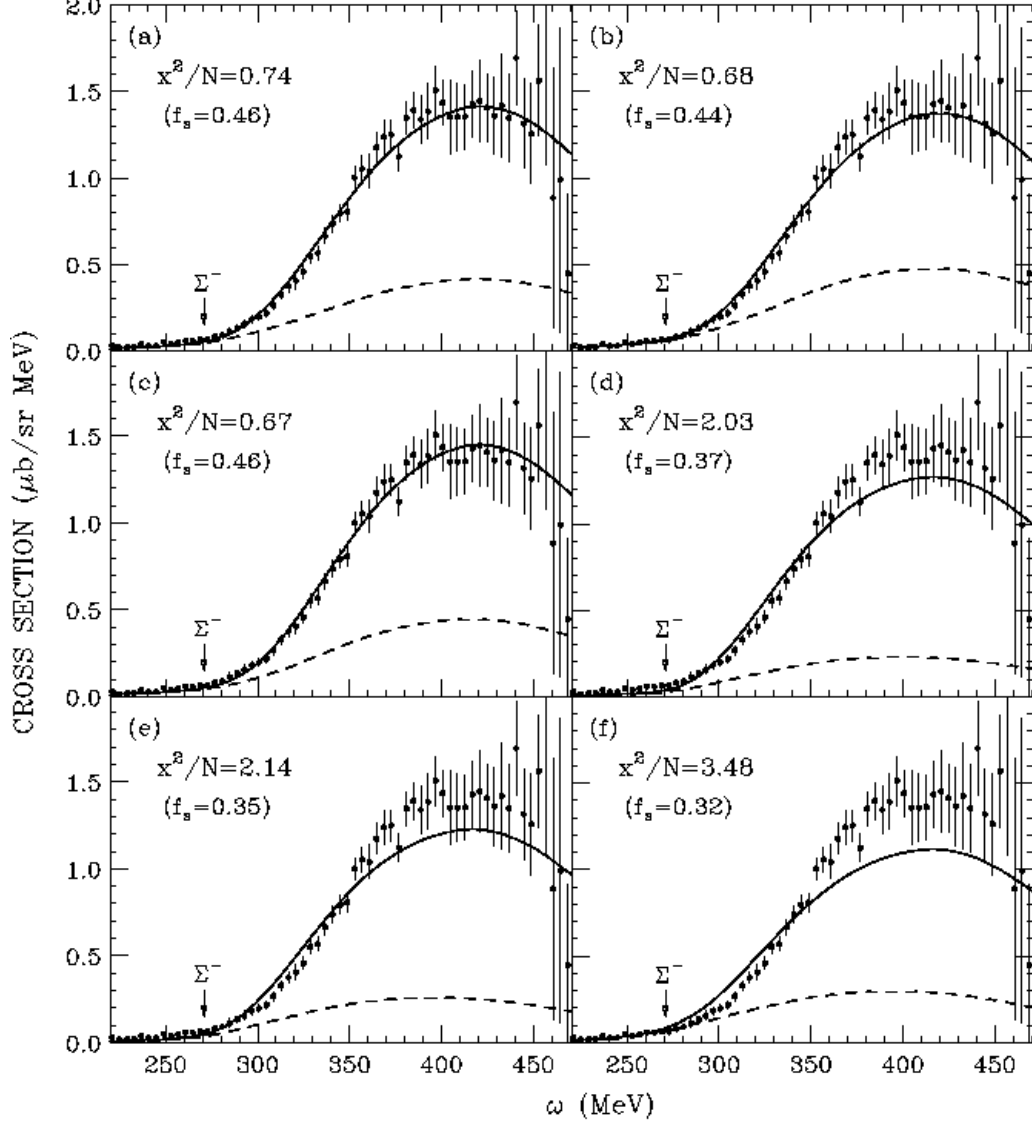


FIG. 16: Comparison between DWIA calculations [90] and the measured $^{28}\text{Si}(\pi^-, K^+)$ spectrum [74] using six Σ -nucleus potentials, (a)-(c) with inner repulsion, (d)-(f) fully attractive. The solid and dashed curves denote the inclusive and Λ conversion cross sections, respectively. Each calculated spectrum was normalized by a fraction f_s . The arrows mark the $\Sigma^- - ^{27}\text{Al}_{\text{g.s.}}$ threshold at $\omega = 270.75$ MeV.

(repulsive) real part and $W_0 = -40$ MeV for the imaginary part. These and other spectra measured on lighter targets suggest that a strongly *repulsive* Σ -nucleus potential is required to reproduce the shape of the inclusive spectrum, while the sensitivity to the imaginary (absorptive) component is secondary. The favored strength of the repulsive potential in this analysis is about 100 MeV, of the same order of magnitude reached by the DD Σ^- atomic fit potential shown in Fig. 13 as it ‘enters’ the nucleus inward. The general level of agreement in the fit shown in Fig. 15 is satisfactory, but there seems to be a systematic effect calling for more repulsion, the heavier is the target. We conclude that a strong evidence has been finally established for the repulsive nature of the Σ -nucleus potential.

More sophisticated theoretical analyses of these KEK (π^-, K^+) spectra [90, 91, 92, 93]

have also concluded that the Σ -nuclear potential is repulsive within the nuclear volume, although they yield a weaker repulsion in the range of 10-40 MeV. An example of a recent analysis of the Si spectrum is shown in Fig. 16 from Ref. [90] where six different Σ -nucleus potentials are tested for their ability within the Distorted Wave Impulse Approximation (DWIA) to reproduce the measured $^{28}\text{Si}(\pi^-, K^+)$ spectrum [74]. This particular DWIA version was tested on the well understood $^{28}\text{Si}(\pi^+, K^+)$ quasi-free Λ hypernuclear spectrum also taken at KEK with incoming pions of the same momentum $p_{\text{lab}} = 1.2 \text{ GeV}/c$. Potential (a) is the DD, type A' potential of Ref. [77], (b) is one of the RMF potentials of Ref. [78], that with $\alpha_\omega = 1$, and (c) is a local-density approximation version of a G matrix constructed from the Nijmegen model F. These three potentials are repulsive within the nucleus but differ considerably there from each other. Potentials (d)-(f) are all attractive within the nucleus, with (f) being of a $t_{\text{eff}}\rho$ form. All of the six potentials are attractive outside the nucleus, as required by fits to the 'attractive' Σ^- atomic level shifts. The figure shows clearly, and judging by the associated χ^2/N values, that fully attractive potentials are ruled out by the data and that only the '*repulsive*' Σ -nucleus potentials reproduce the spectrum very well, but without giving preference to any of these potentials (a)-(c) over the other ones in this group. It was shown by Harada and Hirabayashi [93], furthermore, that the (π^-, K^+) data on targets with neutron excess, such as ^{209}Bi , also lack the sensitivity to confirm the presence of a sizable (repulsive for Σ^-) isovector component of the Σ nucleus interaction as found in the Σ^- -atom fits [76, 77, 78].

Acknowledgments

Special thanks are due to the Directors of Course CLXVII 'strangeness and spin in fundamental physics' Mauro Anselmino and Tullio Bressani, to the Scientific Secretary Alessandro Feliciello and to the School Secretary Ms. Barbara Alzani and her crew. This Review was supported in part by the Israel Science Foundation grant 757/05.

-
- [1] C.J. Batty, E. Friedman, A. Gal, Phys. Rep. **287** (1997) 385.
 - [2] E. Friedman, A. Gal, Phys. Rep. **452** (2007) 89.
 - [3] D. Gotta, Prog. Part. Nucl. Phys. **52** (2004) 133.
 - [4] A. Trzcińska, J. Jastrzębski, P. Lubiński, F.J. Hartmann, R. Schmidt, T. von Egidy, B. Kłos, Phys. Rev. Lett. **87** (2001) 082501.
 - [5] J. Jastrzębski, A. Trzcińska, P. Lubiński, B. Kłos, F.J. Hartmann, T. von Egidy, S. Wycech, Int. J. Mod. Phys. E **13** (2004) 343.
 - [6] E. Friedman, A. Gal, J. Mareš, Nucl. Phys. A **761** (2005) 283.
 - [7] N. Barnea, E. Friedman, Phys. Rev. C **75** (2007) 022202(R).
 - [8] G. Fricke, C. Bernhardt, K. Heilig, L.A. Schaller, L. Schellenberg, E.B. Shera, C.W. De Jager, Atom. Data Nucl. Data Tables **60** (1995) 177.
 - [9] M. Krell, Phys. Rev. Lett. **26** (1971) 584.
 - [10] Gal, E. Friedman and C.J. Batty, Nucl. Phys. A **606** (1996) 283.
 - [11] J. Mareš, E. Friedman, A. Gal, Nucl. Phys. A **770** (2006) 84.
 - [12] A. Baca, C. García-Recio, J. Nieves, Nucl. Phys. A **673** (2000) 335.
 - [13] C.J. Batty, E. Friedman, H.J. Gils, H. Rebel, Adv. Nucl. Phys. **19** (1989) 1.

- [14] A. Ramos, E. Oset, Nucl. Phys. A **671** (2000) 481.
- [15] A. Cieplý, E. Friedman, A. Gal, J. Mareš, Nucl. Phys. A **696** (2001) 173.
- [16] T. Waas, N. Kaiser, W. Weise, Phys. Lett. B **379** (1996) 34.
- [17] E. Friedman, A. Gal, Phys. Lett. B **459** (1999) 43.
- [18] E. Friedman, A. Gal, Nucl. Phys. A **658** (1999) 345.
- [19] C.J. Batty, E. Friedman, A. Gal, Nucl. Phys. A **689** (2001) 721.
- [20] R.H. Dalitz, S.F. Tuan, Phys. Rev. Lett. **2** (1959) 425.
- [21] B. Borasoy, R. Nißler, W. Weise, Phys. Rev. Lett. **94** (2005) 213401.
- [22] B. Borasoy, R. Nißler, W. Weise, Eur. Phys. J. A **25** (2005) 79.
- [23] B. Borasoy, R. Nißler, W. Weise, Phys. Rev. Lett. **96** (2006) 199201.
- [24] B. Borasoy, U.-G. Meißner, R. Nißler, Phys. Rev. C **74** (2006) 055201.
- [25] G. Beer et al. [DEAR Collaboration], Phys. Rev. Lett. **94** (2005) 212302.
- [26] W. Weise, arXiv:nucl-th/0701035, plenary talk at HYP06, Mainz, October 2006.
- [27] T. Waas, M. Rho, W. Weise, Nucl. Phys. A **617** (1997) 449, and references therein.
- [28] J. Schaffner-Bielich, V. Koch, M. Effenberger, Nucl. Phys. A **669** (2000) 153.
- [29] L. Tolos, A. Ramos, A. Polls, T.T.S. Kuo, Nucl. Phys. A **690** (2001) 547.
- [30] E.G. Drukarev, private communication, May 2006.
- [31] J. Schaffner, A. Gal, I.N. Mishustin, H. Stöcker, W. Greiner, Phys. Lett. B **334** (1994) 268.
- [32] G.E. Brown, M. Rho, Nucl. Phys. A **596** (1996) 503.
- [33] W. Scheinast et al., Phys. Rev. Lett. **96** (2006) 072301, and references therein.
- [34] Y. Nogami, Phys. Lett. **7** (1963) 288.
- [35] T. Yamazaki, Y. Akaishi, Phys. Lett. B **535** (2002) 70.
- [36] A. Doté, W. Weise, arXiv:nucl-th/0701050, presented at HYP06, Mainz, October 2006.
- [37] N.V. Shevchenko, A. Gal, J. Mareš, Phys. Rev. Lett. **98** (2007) 082301.
- [38] N.V. Shevchenko, A. Gal, J. Mareš, J. Révai, Phys. Rev. C **76** (2007) 044004.
- [39] Y. Ikeda, T. Sato, arXiv:nucl-th/0701001, presented at HYP06, Mainz, October 2006.
- [40] Y. Ikeda, T. Sato, Phys. Rev. C **76** (2007) 035203.
- [41] M. Agnello et al. [FINUDA Collaboration], Phys. Rev. Lett. **94** (2005) 212303.
- [42] V.K. Magas, E. Oset, A. Ramos, H. Toki, Phys. Rev. C **74** (2006) 025206.
- [43] M. Agnello et al. [FINUDA Collaboration], Nucl. Phys. A **775** (2006) 35.
- [44] G. Bendiscioli, T. Bressani, A. Fontana, L. Lavezzi, A. Panzarasa, A. Rotondi, Nucl. Phys. A **789** (2007) 222.
- [45] T. Nagae, in *Topics in Strangeness Nuclear Physics*, Eds. P. Bydžovský, A. Gal, J. Mareš, Lecture Notes in Physics **724** (Springer, Berlin Heidelberg 2007) pp. 81-111.
- [46] T. Koike, T. Harada, Phys. Lett. B **652** 262.
- [47] T. Kishimoto, Phys. Rev. Lett. **83** (1999) 4701.
- [48] Y. Akaishi, T. Yamazaki, in: S. Bianconi, et al. (Eds.), Proc. III Int. DAΦNE Workshop, Frascati Physics Series vol. XVI, LNF, Frascati, 1999, pp. 59-74.
- [49] Y. Akaishi, T. Yamazaki, Phys. Rev. C **65** (2002) 044005.
- [50] S. Wycech, Nucl. Phys. A **450** (1986) 399c.
- [51] M. Iwasaki et al. [KEK E549/570 Collaboration], arXiv:0706.0297 [nucl-ex], plenary talk given by M. Iwasaki at HYP06, Mainz, October 2006.
- [52] M. Sato et al. [KEK E549 Collaboration], arXiv:0708.2968 [nucl-ex], submitted to Phys. Lett. B.
- [53] M. Agnello et al. [FINUDA Collaboration], Phys. Lett. B **654** (2007) 80.
- [54] T. Suzuki et al. [KEK E549 Collaboration], arXiv:0709.0996 [nucl-ex], submitted to Phys.

Rev. Lett.

- [55] T. Kishimoto et al. [AGS E930 Collaboration], Nucl. Phys. A **754** (2005) 383c.
- [56] T. Kishimoto et al. [KEK E548 Collaboration], Prog. Theor. Phys. **118** (2007) 181.
- [57] J. Mareš, E. Friedman, A. Gal, Phys. Lett. B **606** (2005) 295.
- [58] D. Gazda, E. Friedman, A. Gal, J. Mareš, Phys. Rev. C (in press).
- [59] E. Friedman, A. Gal, J. Mareš, A. Cieplý, Phys. Rev. C **60** (1999) 024314.
- [60] M.M. Sharma, M.A. Nagarajan, P. Ring, Phys. Lett. B **312** (1993) 377.
- [61] B.D. Kaplan, A.E. Nelson, Phys. Lett. B **175** (1986) 57.
- [62] A.E. Nelson, B.D. Kaplan, Phys. Lett. B **192** (1987) 193.
- [63] G.E. Brown, C.-H. Lee, M. Rho, V. Thorsson, Nucl. Phys. A **567** (1994) 937.
- [64] C.-H. Lee, G.E. Brown, D.-P. Min, M. Rho, Nucl. Phys. A **585** (1995) 401.
- [65] J. Schaffner-Bielich, A. Gal, Phys. Rev. C **62** (2000) 034311.
- [66] C.B. Dover, A. Gal, Prog. Part. Nucl. Phys. **12** (1984) 171.
- [67] Th.A. Rijken, Y. Yamamoto, Phys. Rev. C **73** (2006) 044008.
- [68] C.J. Batty, Phys. Lett. **87B** (1979) 324.
- [69] C.J. Batty, A. Gal, G. Toker, Nucl. Phys. A **402** (1983) 349.
- [70] C.B. Dover, D.J. Millener, A. Gal, Phys. Rep. **184** (1989) 1.
- [71] S. Bart et al., Phys. Rev. Lett. **83** (1999) 5238.
- [72] J. Dabrowski, Phys. Rev. C **60** (1999) 025205.
- [73] H. Noumi et al. [KEK E438 Collaboration], Phys. Rev. Lett. **89** (2002) 072301; *ibid.* **90** (2003) 049902(E).
- [74] P.K. Saha et al. [KEK E438 Collaboration], Phys. Rev. C **70** (2004) 044613.
- [75] R.J. Powers et al. [AGS E723 Collaboration], Phys. Rev. C **47** (1993) 1263.
- [76] C.J. Batty, E. Friedman, A. Gal, Phys. Lett. B **335** (1994) 273.
- [77] C.J. Batty, E. Friedman, A. Gal, Prog. Theor. Phys. Suppl. **117** (1994) 227.
- [78] J. Mareš, E. Friedman, A. Gal, B.K. Jennings, Nucl. Phys. A **594** (1995) 311.
- [79] S. Balberg, A. Gal, Nucl. Phys. A **625** (1997) 435.
- [80] J. Haidenbauer, Ulf-G. Meissner, Phys. Rev. C **72** (2005) 044005.
- [81] M. Kohno, Y. Fujiwara, T. Fujita, C. Nakamoto, Y. Suzuki, Nucl. Phys. A **674** (2000) 229.
- [82] N. Kaiser, Phys. Rev. C **71** (2005) 068201.
- [83] J. Schaffner, I.N. Mishustin, Phys. Rev. C **53** (1996) 1416.
- [84] J. Schaffner-Bielich, arXiv:astro-ph/0703113, plenary talk at HYP06, Mainz, October 2006.
- [85] A. Ramos, J. Schaffner-Bielich, J. Wambach, Lect. Notes Phys. **578** (2001) pp. 175-202.
- [86] R.S. Hayano, T. Ishikawa, M. Iwasaki, H. Outa, E. Takada, H. Tamura, A. Sakaguchi, M. Aoki, T. Yamazaki, Phys. Lett. B **231** (1989) 355.
- [87] T. Harada, S. Shinmura, Y. Akaishi, H. Tanaka, Nucl. Phys. A **507** (1990) 715.
- [88] T. Nagae et al. [AGS E905 Collaboration], Phys. Rev. Lett. **80** (1998) 1605.
- [89] T. Harada, Phys. Rev. Lett. **81** (1998) 5287.
- [90] T. Harada, Y. Hirabayashi, Nucl. Phys. A **759** (2005) 143.
- [91] M. Kohno, Y. Fujiwara, Y. Watanabe, K. Ogata, M. Kawai, Prog. Theor. Phys. **112** (2004) 895.
- [92] M. Kohno, Y. Fujiwara, Y. Watanabe, K. Ogata, M. Kawai, Phys. Rev. C **74** (2006) 064613.
- [93] T. Harada, Y. Hirabayashi, Nucl. Phys. A **767** (2006) 206.